LBL-36755
UC-413
Preprint

Lawrence Berkeley Laboratory
UNIVERSITY OF CALIFORNIA

Submitted to Nuclear Physics B

QCD Mechanisms for Double Quarkonium and Open Heavy Meson Hadroproduction

R. Vogt

March 1995

U. C. Lawrence Berkeley Laboratory
Library, Berkeley

FOR REFERENCE

Not to be taken from this room

REFERENCE COPY
Does Not
Circulate
Bldg. 50 Library.
LBL-36755
Copy 1

Prepared for the U.S. Department of Energy under Contract Number DE-AC03-76SF00098

DISCLAIMER

This document was prepared as an account of work sponsored by the United States Government. While this document is believed to contain correct information, neither the United States Government nor any agency thereof, nor the Regents of the University of California, nor any of their employees, makes any warranty, express or implied, or assumes any legal responsibility for the accuracy, completeness, or usefulness of any information, apparatus, product, or process disclosed, or represents that its use would not infringe privately owned rights. Reference herein to any specific commercial product, process, or service by its trade name, trademark, manufacturer, or otherwise, does not necessarily constitute or imply its endorsement, recommendation, or favoring by the United States Government or any agency thereof, or the Regents of the University of California. The views and opinions of authors expressed herein do not necessarily state or reflect those of the United States Government or any agency thereof or the Regents of the University of California.

LBL-36755
UC-413

QCD Mechanisms for Double Quarkonium and Open Heavy Meson Hadroproduction

R. Vogt

Nuclear Science Division
Lawrence Berkeley Laboratory
University of California
Berkeley, California 94720

and

Institute for Nuclear Theory
University of Washington
Seattle, Washington 98195

March 1995

This work was supported in part by the Director, Office of Energy Research, Division of Nuclear Physics of the Office of High Energy and Nuclear Physics, of the U.S. Department of Energy under Contract No. DE-AC03-76SF00098.

Nuclear Physics B LBL-36755

QCD Mechanisms for Double Quarkonium and Open Heavy Meson Hadroproduction*

R. Vogt

Nuclear Science Division, Lawrence Berkeley Laboratory, Berkeley, CA 94720
and
Institute for Nuclear Theory, University of Washington, Seattle, WA 98195

March 2, 1995

Abstract:

Double J/ψ production on the order of 20-30 pb has been observed by the NA3 collaboration. These $\psi\psi$ pairs, measured in $\pi^- N$ interactions at 150 and 280 GeV/c and in pN interactions at 400 GeV/c, carry a large fraction of the projectile momentum, $x_{\psi\psi} \geq 0.6$ for the 150 GeV/c beam and ≥ 0.4 at 280 GeV/c. We examine several sources of $\psi\psi$ pair production within QCD, including $\mathcal{O}(\alpha_s^4)$ $\psi\psi$ production, leading-twist $b\bar{b}$ production and decay, and the materialization of heavy-quark Fock states in the projectile. We estimate the production cross section and the single and double J/ψ momentum and mass distributions for each, comparing the results with the NA3 data, and predict $\psi\psi$ production in pN interactions at 800 GeV/c, accessible to current fixed-target experiments. We also discuss the observable implications of open heavy meson pair production from the intrinsic heavy quark Fock states.

*This work was supported in part by the Director, Office of Energy Research, Division of Nuclear Physics of the Office of High Energy and Nuclear Physics of the U. S. Department of Energy under Contract Number DE-AC03-76SF0098.

I. Introduction

The production of charmonium pairs in the same reaction is expected to be exceedingly rare in QCD. However, the NA3 collaboration has measured $\psi\psi$ pair production in multi-muon events in π^-Pt interactions at 150 and 280 GeV [1] and in 400 GeV pPt interactions [2]. The integrated $\psi\psi$ production cross section per nucleon, $\sigma_{\psi\psi}$, is 18 ± 8 pb at 150 GeV and 30 ± 10 pb at 280 GeV for pion-induced and 27 ± 10 pb proton-induced interactions at 400 GeV. This cross section is reduced relative to the single J/ψ production cross section, σ_ψ, by $\sigma_{\psi\psi}/\sigma_\psi \approx (3 \pm 1) \times 10^{-4}$ in the pion-induced events.

The fraction of the projectile momentum, $x_{\psi\psi} = p_{\rm lab}^{\psi\psi}/p_{\rm beam}$, carried by the $\psi\psi$ pair is always very large, $x_{\psi\psi} \geq 0.6$ at 150 GeV and $x_{\psi\psi} \geq 0.4$ at 280 GeV. Additionally, single J/ψ mesons in the $\psi\psi$ pairs have $x_\psi > 0.15$. When the data from both pion beams are combined, $\langle x_{\psi\psi}\rangle = 0.66$ and $\langle x_\psi\rangle = 0.33$. As we shall show, perturbative gg and $q\bar{q}$ fusion processes produce central $\psi\psi$ pairs with lower average momentum fractions[1]. The average invariant mass of the pair, $\langle M_{\psi\psi}\rangle = 7.4$ GeV, is well above the $\psi\psi$ production threshold, $2m_\psi = 6.2$ GeV. In fact, all of the observed events have an invariant mass greater than 6.7 GeV. Additionally, the average transverse momentum of the pair is quite small, $p_{T,\psi\psi} = 0.9 \pm 0.1$ GeV, suggesting that $\psi\psi$ pair production is highly correlated, occurring in the same interaction. The pN events have a somewhat lower invariant mass, $\langle M_{\psi\psi}\rangle \approx 6.8$ GeV, with several events near threshold. The $x_{\psi\psi}$ distribution was not reported.

In this paper, we shall investigate a number of leading-twist and higher-twist $\psi\psi$ pair production models. Several leading-twist production mechanisms have been discussed previously, including $\mathcal{O}(\alpha_s^4)$ $\psi\psi$ production via gg fusion and $q\bar{q}$ annihilation [3–5], $B\overline{B}$ production and decay, $B\overline{B} \to \psi\psi X$ [6], and the production of a $2^{++}c\bar{c}c\bar{c}$ resonance that decays into $\psi\psi$ pairs [7]. We review double J/ψ hadroproduction by these leading-twist mechanisms, updating the results with more recent parameters and nonscaling parton distributions. These models are unable to produce $\psi\psi$ pairs with large $x_{\psi\psi}$.

We then turn to a higher-twist mechanism that easily produces fast $Q\overline{Q}$ pairs: intrinsic heavy quark components in the projectile wavefunction [8]. In a companion paper, Ref. [9], we evaluated the probability for two J/ψ's to originate from an intrinsic $|\bar{u}dc\bar{c}c\bar{c}\rangle$ Fock state. This model was successful in reproducing the general features of the data. In this paper, we also consider several other sources of double J/ψ production by intrinsic heavy quark states. An intrinsic $b\bar{b}$ pair, $|\bar{u}db\bar{b}\rangle$, could decay into $\psi\psi$ pairs, as in leading-twist $b\bar{b}$ production. Additionally, an intrinsic $|\bar{u}dc\bar{c}b\bar{b}\rangle$ state could produce $\psi\psi$ pairs from a $B \to J/\psi X$ decay combined with the coalescence of the $c\bar{c}$ pair into a J/ψ. Finally, we calculate $\psi\psi$ pair production through leading-twist $c\bar{c}$ production with the projectile in an intrinsic $c\bar{c}$ state. Examples of all the processes considered are shown in Fig. 1.

In addition to estimating the $\psi\psi$ production cross section for all of the leading-twist and higher-twist mechanisms, we compare our results to the combined NA3 pion-induced data and the invariant mass distribution from the 400 GeV proton-induced production. We also discuss $\psi\psi$ pair production by 800 GeV proton beams, measurable in ongoing fixed-target experiments. To facilitate comparison with the data, we present all the momentum distributions in the laboratory frame and normalize the pion-induced calculations to the combined 150 and 280 GeV data and the proton-induced calculations to the 400 GeV data. The $\psi\psi$ pair mass and momentum distributions are normalized to the pair rate while the J/ψ momentum distributions are normalized to the single rate, twice the pair rate.

II. Leading-Twist Production Mechanisms

In this section we shall review the leading-twist QCD predictions for double quarkonium hadroproduction, $\mathcal{O}(\alpha_s^4)$ $\psi\psi$ production and $b\bar{b}$ production and decay. We also estimate double J/ψ production assuming the existence of a $2^{++}c\bar{c}c\bar{c}$ resonance. These processes are sensitive to the parton distributions in the pion and nucleon. We use two sets of recent leading-order parton distribution functions in our calculations, GRV LO, available for both nucleons [10] and pions [11], and Duke-Owens 1.1 [12] for the nucleon with Owens I [13] for the pion. The results we present are calculated for a proton target, but at these energies and with these scale choices, the π^-p cross sections can be $\approx 50\%$ larger than the corresponding π^-N cross sections since the contribution from pion valence quark annihilation is important. There is no significant difference between the pp and pN production cross sections.

Since the calculations are leading order, a K factor is usually invoked to account for next-to-leading order corrections. For example, in $b\bar{b}$ production, $K = \sigma(\alpha_s^3)/\sigma(\alpha_s^2) \approx 1.2 - 2.5$, depending on the choice of m_b and the scale parameter

[1]Single J/ψ's produced at rest in the π^-N center of mass have laboratory momentum fractions of $x_\psi = 0.18$ at 150 GeV and 0.14 at 280 GeV. Likewise, assuming $M_{\psi\psi} = 7$ GeV leads to laboratory fractions $x_{\psi\psi} = 0.42$ at 150 GeV and 0.3 at 280 GeV for $\psi\psi$ pairs at rest in the π^-N center of mass.

μ_b [14]. Indeed, for $\mu_b = m_b$, $\sigma(m_b = 4.5\,\mathrm{GeV})/\sigma(m_b = 5\,\mathrm{GeV}) \approx 3.7$ at $\mathcal{O}(\alpha_s^2)$ while for $m_b = 4.75$ GeV, $\sigma(\mu_b = 0.5m_b)/\sigma(\mu_b = 2m_b) \approx 6$ at $\mathcal{O}(\alpha_s^2)$ and 3 at $\mathcal{O}(\alpha_s^3)$. Thus over a reasonable range of m_b and μ_b, the leading order $b\bar{b}$ production cross section can vary by an order of magnitude at the energies studied here.

There is thus considerable uncertainty in the normalization of the leading-twist $\psi\psi$ production cross section. In our analysis we will quote a representative value of $\sigma_{\psi\psi}$. The most important test of these models, however, is the shape of the momentum and invariant mass distributions since these are not strongly affected by the target type or the scale parameters. We will find that while some of these mechanisms can account for the magnitude of $\sigma_{\psi\psi}$ within a factor of 2-3, none of them can fully describe the characteristics of the momentum and invariant mass distributions.

1. Production at $\mathcal{O}(\alpha_s^4)$

Leading-twist double J/ψ production has been calculated to leading order in α_s, $\mathcal{O}(\alpha_s^4)$, in Ref. [3–5]. In these caclculations, the J/ψ's are treated as nonrelativistic bound states with the appropriate spin and angular momentum quantum numbers, as in the color-singlet model of quarkonium production [15]. Examples of $gg \to \psi\psi$ production diagrams are shown in Fig. 1(a). There are 36 diagrams in all, some vanish due to color conservation and others can be related by crossing [4]. The $q\bar{q} \to \psi\psi$ diagrams [3,4] are shown in Fig. 1(b). After four-momentum conservation is accounted for, the $\mathcal{O}(\alpha_s^4)$ $\psi\psi$ production cross section may be written as

$$\frac{d\sigma}{dp_T^2 dy_Q dy_{\overline{Q}}} = \sum_q (F_q(x_1)F_{\bar{q}}(x_2) + F_{\bar{q}}(x_1)F_q(x_2))\frac{d\hat{\sigma}}{d\hat{t}}|_{q\bar{q}} + F_g(x_1)F_g(x_2)\frac{d\hat{\sigma}}{d\hat{t}}|_{gg} \ , \tag{1}$$

where $x_1 = m_{T,\psi}(e^{y_1}+e^{y_2})/\sqrt{s}$, $x_2 = m_{T,\psi}(e^{-y_1}+e^{-y_2})/\sqrt{s}$ and $m_{T,\psi}^2 = m_\psi^2 + p_T^2$. The parton momentum distribution functions, $F(x) = xG(x)$, are evolved to $Q^2 = 4m_\psi^2$ so that when the renormalization and factorization scales are assumed to be equal, $\alpha_s \approx 0.21$.

The subprocess cross sections for $\psi\psi$ production to order $\mathcal{O}(\alpha_s^4)$ from $q\bar{q}$ annihilation and gg fusion are [4]

$$\frac{d\hat{\sigma}}{d\hat{t}}|_{q\bar{q}} = \frac{2}{3\pi}\left(\frac{16\pi\alpha_s}{3}\right)^4 \frac{|\Psi(0)|^2}{m_\psi}\frac{|\Psi(0)|^2}{m_\psi}\frac{1}{\hat{s}^4}[3 + 4y - 10z^2 - 24z^2y - 24z^4] \ , \tag{2}$$

$$\frac{d\hat{\sigma}}{d\hat{t}}|_{gg} = \frac{3}{4\pi}\left(\frac{\pi\alpha_s}{3}\right)^4 \frac{|\Psi(0)|^2}{m_\psi}\frac{|\Psi(0)|^2}{m_\psi}\frac{\hat{s}^4\sum_0^4 y^n C_n(z)}{(\hat{t}-m_\psi^2)^4(\hat{u}-m_\psi^2)^4} \ , \tag{3}$$

where $y = (\hat{t}+\hat{u})/2\hat{s}$, $z = (\hat{t}-\hat{u})/2\hat{s}$ and $\hat{s} = x_a x_b s$, $\hat{t} = -x_1 m_{T,\psi}\sqrt{s}e^{-y_1} + m_\psi^2$, and $\hat{u} = -x_2 m_{T,\psi}\sqrt{s}e^{y_1} + m_\psi^2$. The J/ψ wavefunction at the origin, $|\Psi(0)|^2$, is fixed by the electromagnetic decay width, $\Gamma(J/\psi \to e^+e^-)$. We use the most recent determination, $|\Psi(0)|^2 = 0.0689$ GeV^3 [16]. The polynomials $C_n(z)$, from Ref. [4], are

$$\begin{aligned}
C_0 &= \frac{2}{3}(3981312z^{12} + 258048z^{10} - 1186048z^8 + 35584z^6 \\
&\quad + 98144z^4 - 13568z^2 + 335) \\
C_1 &= \frac{8}{3}(1935360z^{10} - 596224z^8 - 403840z^6 + 168084z^4 \\
&\quad - 14288z^2 + 137) \\
C_2 &= \frac{8}{3}(1134336z^8 - 1010944z^6 + 239008z^4 - 11472z^2 - 1) \\
C_3 &= \frac{64}{3}(-10176z^6 + 688z^4 + 828z^2 + 5) \\
C_4 &= 26(16z^4 + 8z^2 + 1) \ .
\end{aligned}$$

The predicted cross sections for $\pi^-p \to \psi\psi$ are 7.4 pb at 150 GeV and 16.5 pb at 280 GeV, $\approx$ 30-50% of the measured total. At 400 GeV, the predicted $pp \to \psi\psi$ production cross section is 7.2 pb, $\approx$ 30% below the data, increasing to 26 pb at 800 GeV [2].

---

[2] In Ref. [4], a smaller value of the wavefunction, $|\Psi(0)|^2 = 0.0387$ GeV^3, and a larger value of the strong coupling constant, $\alpha_s = 0.32$, were used, leading to similar conclusions about the magnitude of the production cross section.

The calculations are compared with the $\pi^- N \to \psi\psi X$ data in Fig. 2. The results are not strongly dependent on the choice of parton distributions. The momentum distributions are relatively broad, with $\langle x_\psi \rangle = 0.26$ and $\langle x_{\psi\psi} \rangle = 0.5$ at 150 GeV; $\langle x_\psi \rangle = 0.21$ and $\langle x_{\psi\psi} \rangle = 0.4$ at 280 GeV. Note that $\langle x_{\psi\psi} \rangle$ is significantly less than required by the $\psi\psi$ data. In fact, all the measured pairs have a larger $x_{\psi\psi}$ than these averages. Also 20% of the single J/ψ's in the pairs have $x_\psi > 0.5$, larger than predicted by leading order QCD $\psi\psi$ production. The $pp \to \psi\psi$ calculations, shown in Fig. 3, predict narrower distributions than the $\pi^- p$ calculations: $\langle x_\psi \rangle = 0.15$ and $\langle x_{\psi\psi} \rangle = 0.3$ at 400 GeV; $\langle x_\psi \rangle = 0.11$ and $\langle x_{\psi\psi} \rangle = 0.24$ at 800 GeV. We find $\langle M_{\psi\psi} \rangle = 7$ GeV for both projectiles. This is in good agreement with the 400 GeV proton-induced data where the pair mass is low. However, the $\pi^- N$ data suggests that production occurs above threshold. Thus although the absolute cross sections are not significantly below the data, the mass and longitudinal momentum distributions from this model fail to describe the data.

2. Leading-Twist $b\bar{b}$ Production

We estimate the $\psi\psi$ pair production cross section from leading-twist $b\bar{b}$ production and decay. At $\mathcal{O}(\alpha_s^2)$, $b\bar{b}$ production proceeds by gg fusion and $q\bar{q}$ annihilation, as shown in Fig. 1(c). The $b\bar{b}$ production cross section has the same form as Eq. (1) but the subprocess cross sections are [17]

$$\frac{d\hat{\sigma}}{d\hat{t}}|_{q\bar{q}} = \frac{\pi\alpha_s^2}{9\hat{m}_b^4} \frac{\cosh(y_b - y_{\bar{b}}) + m_b^2/\hat{m}_b^2}{(1+\cosh(y_b - y_{\bar{b}}))^3} , \tag{4}$$

$$\frac{d\hat{\sigma}}{d\hat{t}}|_{gg} = \frac{\pi\alpha_s^2}{96\hat{m}_b^4} \frac{8\cosh(y_b - y_{\bar{b}}) - 1}{(1+\cosh(y_b - y_{\bar{b}}))^3} \left(\cosh(y_b - y_{\bar{b}}) + \frac{2m_b^2}{\hat{m}_b^2} - \frac{2m_b^4}{\hat{m}_b^4} \right) . \tag{5}$$

The parton distributions are evaluated at $Q^2 = 4m_b^2$ with $m_b = 4.75$ GeV. The predicted rates of open $b\bar{b}$ production are $\sigma_{b\bar{b}}^{\rm tot}(\pi^- p) = 230$ pb at 150 GeV and 2 nb at 280 GeV. We also find $\sigma_{b\bar{b}}^{\rm tot}(pp) = 250$ pb at 400 GeV and 1.3 nb at 800 GeV. As previously discussed, changing m_b and $Q = \mu_b$ can change the predicted $\sigma_{b\bar{b}}^{\rm tot}$ by a factor of five to ten.

Flavor excitation has been considered as a source of b quark production in Ref. [6]. These quark-gluon scattering graphs are considered part of the K factor which increases the cross section by $K \approx 2$ [17], as already discussed. In fact, if the uncertainties are varied to produce the maximum production rate, the $\pi^- p$ production cross section could be increased to ≈ 10 nb, not the 100 nb predicted in Ref. [6]. A later study [4] ruled out $b\bar{b}$ production as a significant source of $\psi\psi$ pair production due to the small production cross section, further reduced by the $B\overline{B} \to \psi\psi$ decay. Indeed, including the square of the inclusive branching ratio, $BR(B \to J/\psi X) \approx 1.3\%$, [18] the results are a factor of 10 to 100 below the data[3]. Our predicted $\pi^- p \to \psi\psi$ production cross sections are then 0.028 pb at 150 GeV and 0.24 pb at 280 GeV while the corresponding $pp \to \psi\psi$ cross sections are 0.03 pb at 400 GeV and 0.16 pb at 800 GeV.

Measurements of charm hadroproduction show that the longitudinal momentum distribution of final-state D mesons are similar to the predicted charmed quark distributions. Using a fragmentation function that reproduces D production in e^+e^- annihilation [19] softens the D distribution further. However, in hadroproduction, comoving light partons can combine with the charmed quarks without significant momentum loss by the charmed quark so that the fragmentation can be described by a delta function, $D_{D/c}(z) \approx \delta(z-1)$, in matter [20]. Since the b quark fragmentation function from e^+e^- annihilation predicts less momentum loss [21], the delta function approximation of fragmentation should be even better for b quarks. Therefore $x_{B\overline{B}} = x_{b\bar{b}}$ and $x_B = x_b$. However, the mass distributions are kinematically affected since the B meson mass reduces the available phase space for high mass $B\overline{B}$ pairs. We find that the average $B\overline{B}$ mass is approximately 1 GeV larger than the average $b\bar{b}$ mass and that both increase with incident energy. This predicts a larger $\psi\psi$ invariant mass than $\mathcal{O}(\alpha_s^4)$ $\psi\psi$ production since each J/ψ is produced by an isotropic decay, leading to a larger rapidity gap between the J/ψ's and thus higher $\psi\psi$ pair masses. Note that the $\psi\psi$ pair masses are larger if the b quarks are assumed to decay into J/ψ's directly. However, the single and pair J/ψ distributions are only weakly dependent on whether the parent particle was a b quark or a B meson. The x_ψ and $x_{\psi\psi}$ J/ψ distributions have larger average values and narrower widths than the $\mathcal{O}(\alpha_s^4)$ calculations.

---

[3]We assume that all b quarks produce final states that can decay to J/ψ's to get an upper bound on the $\psi\psi$ production cross section and study inclusive B decays. Choosing an exclusive decay channel, such as $B \to J/\psi K$, reduces the branching ratio. Other assumptions of how the final-state hadrons are produced would also reduce the J/ψ rate.

We calculate the $B \to J/\psi X$ decay distributions by a Monte Carlo using J/ψ momentum distributions calibrated to the B decays measured at CLEO [22]. The J/ψ and $\psi\psi$ distributions are not smooth due to the finite statistics of the Monte Carlo.

The B and J/ψ laboratory frame distributions are given in Figs. 4 and 5. The B and $B\overline{B}$ longitudinal momentum distributions are calculated with both sets of parton distribution functions. The invariant mass, J/ψ and $\psi\psi$ momentum distributions are shown for the GRV LO partons only to illustrate the differences arising from assuming either that the b quarks decay directly to J/ψ or that the quarks first hadronize and then decay. The average momentum fractions and invariant masses of the B mesons and J/ψ's calculated with the GRV LO parton distributions are shown in Table I. In addition to the shape differences between the calculations and the data, the predicted normalization is a factor of ≈ 100 smaller than required by the data. Thus we can conclude that leading-twist $b\bar{b}$ production is not an important source of $\psi\psi$ production at these energies.

3. $2^{++}c\bar{c}c\bar{c}$ Resonance Production

In the resonance model of Ref. [7], $\psi\psi$ pairs with $M_{\psi\psi} \equiv 7$ GeV are produced by a Drell-Yan type mechanism where two gluons fuse in a color vector-meson dominance model. Each gluon couples to a $c\bar{c}$ pair in the color-octet-vector representation. The $c\bar{c}$ pairs then couple to a $2^{++}c\bar{c}c\bar{c}$ state which subsequently decays to $\psi\psi$ pairs. The basic process, which has been generalized to a number of vector-meson final states, is shown in Fig. 1(d). We follow Ref. [7] in our calculations. The $\psi\psi$ pair longitudinal momentum distribution in the laboratory frame is

$$\frac{d\sigma}{dp_{\psi\psi}} = \frac{1}{sp_L}\int_{W^2_{\min}}^{s} dW^2 \frac{2}{\sqrt{z^2 + W^2/p_L^2}} G_g(x_1)G_g(x_2)\sigma_{gg} \ , \tag{6}$$

where $G_g(x)$ represent the gluon number densities, z is the fraction of the laboratory momentum, p_L, carried by the $\psi\psi$ pair, W is the center of mass energy of the two gluons, and $W^2_{\min} = 4m_\psi^2$. The gluon fusion cross section is

$$\sigma_{gg} = \frac{1}{64}\frac{k}{128\pi W}\frac{7}{3}\left(1 + \frac{2k^2}{3m_\psi^2} + \frac{2k^4}{15m_\psi^4}\right)\frac{a_{\psi\psi}^2 b_{\psi\psi}^2}{(W - M_{\psi\psi})^2 + \Gamma_{\psi\psi}^2(W)/4} \ , \tag{7}$$

where $a_{\psi\psi} = a/\sqrt{3}$ is the resonance decay constant, $b_{\psi\psi} = \sqrt{2/3}\alpha_s a(4\pi/f_{\underline{\psi}})^2$ is the coupling between the gluons and the 2^{++} state, $a \simeq \sqrt{30}$, and $(4\pi/f_{\underline{\psi}})^2 \simeq 0.02$, the color vector dominance constant. The width of the $\psi\psi$ resonance is

$$\Gamma_{\psi\psi}(W) = \frac{a^2 k}{24\pi}\left(1 + \frac{2k^2}{3m_\psi^2} + \frac{2k^4}{15m_\psi^4}\right) \ , \tag{8}$$

where $k = 0.5\sqrt{W^2 - 4m_\psi^2}$ is the J/ψ momentum in the center of mass. A single J/ψ in the $\psi\psi$ pair has the laboratory momentum distribution

$$\frac{d\sigma}{dp_\psi} = \frac{1}{s}\int_{W^2_{\min}}^{s} dW^2 \int dz \frac{2\sqrt{1 - v_F^2}}{\sqrt{z^2 + W^2/p_L^2}} G_g(x_1)G_g(x_2)\frac{1}{k}\frac{d\sigma_{gg}}{d\cos\theta} \ , \tag{9}$$

where $v_F = z/\sqrt{z^2 + W^2/p_L^2}$ and the limits on z are determined from the angle, θ, between the J/ψ's, $-1 \leq W(p_\psi - zp_L/2)/(k\sqrt{z^2p_L^2 + W^2}) \leq 1$. The angular distribution resulting from the decay of the 2^{++} state is

$$\begin{aligned}\frac{d\sigma_{gg}}{d\cos\theta} = \frac{1}{64}\frac{k}{128\pi W}\Bigg(&\frac{7}{3} + \frac{k^2}{3m_\psi^2}\left[\frac{19}{3} - 5\cos^2\theta\right] \\ &+ \frac{k^4}{m_\psi^4}\left[\frac{5}{9} - \frac{4}{3}\cos^2\theta + \cos^4\theta\right]\Bigg)\frac{a_{\psi\psi}^2 b_{\psi\psi}^2}{(W - M_{\psi\psi})^2 + \Gamma_{\psi\psi}^2(W)/4} \ .\end{aligned} \tag{10}$$

In the original model of Ref. [7], scale invariant parton distribution functions with $\alpha_s = 0.18$ were used. Repeating the calculation using the same gluon distributions, we find agreement with their results, within one standard deviation

of the measured cross sections[4]. However, if the GRV LO gluon distributions are used at $Q = M_{\psi\psi} = 7$ GeV, the cross sections are reduced significantly. We find 1.7 pb at 150 GeV and 10 pb at 280 GeV for pion-induced production; 12.8 pb at 400 GeV and 55.2 pb at 800 GeV from proton-induced production. The momentum and mass distributions are shown in Figs. 6 and 7. Although the model predicts narrower momentum distributions than the $\mathcal{O}(\alpha_s^4)$ process, the averages are similar. However, neither mechanism produces fast $\psi\psi$ pairs.

III. Higher-Twist Production: Intrinsic Heavy Quark Mechanisms

In the following sections, we will discuss the production of one or two J/ψ's from intrinsic heavy quark states in the projectile wavefunction. The wavefunction of a hadron in QCD can be represented as a superposition of Fock states of quarks and gluons, *e.g.* the π^- wavefunction includes $|\overline{u}d\rangle$, $|\overline{u}dg\rangle$, $|\overline{u}dQ\overline{Q}\rangle$, *etc.* components. (Since our calculations are applied to pion and proton projectiles, we use the notation $|n_V Q\overline{Q}\rangle$ for the heavy quark Fock state where $n_V \equiv \overline{u}d$ for a π^- and uud for a proton.) When the projectile scatters in the target, the coherence of the Fock components is broken and its fluctuations can hadronize [8,23]. For example, intrinsic $c\overline{c}$ fluctuations can be liberated, provided the system is probed during the characteristic time, $\Delta t = 2p_{\rm lab}/M^2_{c\overline{c}}$, that such fluctuations exist.

Microscopically, the intrinsic heavy quark Fock components are generated by virtual interactions such as $gg \to Q\overline{Q}$ where the gluons couple to two or more projectile valence quarks. The probability to produce $Q\overline{Q}$ fluctuations scales as $\alpha_s^2(m_Q^2)/m_Q^2$ relative to leading-twist production [24]. Thus intrinsic heavy quark production is higher twist.

The dominant Fock configurations are not far off shell and thus have minimal invariant mass, $M^2 = \sum_i m_{T,i}^2/x_i$, where $m_{T,i}^2 = k_{T,i}^2 + m_i^2$ is the transverse mass of the $i^{\rm th}$ particle in the configuration. Intrinsic $Q\overline{Q}$ Fock components correspond to configurations with equal rapidity constituents. Thus, unlike sea quarks generated from a single parton, intrinsic heavy quarks carry a large fraction of the parent momentum [8]. In fact, if the intrinsic $Q\overline{Q}$ coalesces into a quarkonium state, the momentum of the two heavy quarks is combined and this final state carries a dominant fraction of the projectile momentum.

There is substantial circumstantial evidence for intrinsic $c\overline{c}$ states. For example, the charm structure function of the proton measured by EMC is significantly larger than predicted by photon-gluon fusion at large x_{Bj} [25]. Leading charm production in πN and hyperon-N collisions also requires a charm source beyond leading twist [26,27]. The NA3 collaboration has also shown that single J/ψ production at large x_F is greater than expected from leading-twist production [28].

The probability distribution for a general n–particle heavy quark Fock state as a function of x and $\vec{k}_T$ is written as

$$\frac{dP_{\rm iQ}}{\prod_{i=1}^n dx_i d^2k_{T,i}} = N_n \alpha_s^4(M_{Q\overline{Q}}) \frac{\delta(\sum_{i=1}^n \vec{k}_{T,i})\delta(1-\sum_{i=1}^n x_i)}{(m_h^2 - \sum_{i=1}^n (m_{T,i}^2/x_i))^2} \ , \tag{11}$$

where N_n, assumed to be slowly varying, normalizes the probability. The assumed constituent quark masses are $m_q = 0.3$ GeV, $m_c = 1.5$ GeV, and $m_b = 4.75$ GeV. While the $\vec{k}_T$ dependence is needed to calculate the mass distributions, an average k_T^2 can be used to calculate the x distributions. Thus, eq. (11) can be simplified to

$$\frac{dP_{\rm iQ}}{dx_i \cdots dx_n} = N_n \alpha_s^4(M_{Q\overline{Q}}) \frac{\delta(1-\sum_{i=1}^n x_i)}{(m_h^2 - \sum_{i=1}^n (\widehat{m}_i^2/x_i))^2} \ , \tag{12}$$

where $\widehat{m}_i^2 = m_i^2 + \langle \vec{k}_{T,i}^2 \rangle$ is the effective transverse mass. Assuming $\langle \vec{k}_{T,i}^2 \rangle$ is proportional to the square of the constituent quark mass, we adopt the effective values $\widehat{m}_c = 1.8$ GeV and $\widehat{m}_q = 0.45$ GeV, as in our previous work [20,29] and use $\widehat{m}_b = 5$ GeV. Note that the resulting x distributions are independent of the Lorentz frame. We will show results involving B decays in the laboratory frame. Eqs. (11) and (12) can be generalized to an arbitrary number of light and heavy partons in the Fock state so that the probability distribution for the production of *e.g.* two heavy quark pairs is,

$$\frac{dP_{\rm iQ_1Q_2}}{\prod_{i=1}^n dx_i d^2k_{T,i}} = N_n \alpha_s^4(M_{Q_1\overline{Q}_1})\alpha_s^4(M_{Q_2\overline{Q}_2}) \frac{\delta(\sum_{i=1}^n \vec{k}_{T,i})\delta(1-\sum_{i=1}^n x_i)}{(m_h^2 - \sum_{i=1}^n (m_{T,i}^2/x_i))^2} \ . \tag{13}$$

---

[4]The gluon convolution was assumed to be $G_{g1}^{h_1}(x_1)G_{g2}^{h_2}(x_2) + G_{g2}^{h_1}(x_1)G_{g1}^{h_2}(x_2)$, twice as large as usual [17]. For consistency with Ref. [7], we included this factor in our calculations. However, this difference should be noted.

The intrinsic $Q\overline{Q}$ production cross section can be related to the probability, $P_{\rm iQ}$, by

$$\sigma_{\rm iQ}(hN) = P_{\rm iQ}\sigma^{\rm in}_{hN}\frac{\mu^2}{4\widehat{m}_Q^2} \ . \tag{14}$$

In their single J/ψ measurements, the NA3 collaboration separated the nuclear dependence into a "hard" contribution with a nearly linear A dependence at low x_F and a contribution scaling as $A^{0.77}$ for πA interactions, characteristic of soft interactions, called "diffractive". The soft interaction scale parameter, $\mu^2 \sim 0.2$ GeV^2, was fixed by the assumption that the diffractive fraction of the total production cross section measured by NA3 [28] is the same for charmonium and charmed hadrons. Therefore, we obtained $\sigma_{\rm ic}(\pi N) \approx 0.5$ μb at 200 GeV and $\sigma_{\rm ic}(pN) \approx 0.7$ μb [27] taking $P_{\rm ic} = 0.3\%$ from an analysis of the EMC charm structure function measurements [25].

1. Production From $|n_V b\bar{b}\rangle$ Fock States

We first examine $\psi\psi$ production from a $|n_V b\bar{b}\rangle$ configuration. Because of the scaling properties of the intrinsic $Q\overline{Q}$ production probability [27] the intrinsic $b\bar{b}$ production cross section is

$$\sigma_{\rm ib}(hN) = \sigma_{\rm ic}(hN)\left(\frac{\widehat{m}_c}{\widehat{m}_b}\frac{\alpha_s(M_{b\bar{b}})}{\alpha_s(M_{c\bar{c}})}\right)^4 \ . \tag{15}$$

Thus $\sigma_{\rm ib}(hN) \approx$ 2-3 nb and

$$\sigma^{\psi\psi}_{\rm ib}(\pi^- N) = [BR(B \to J/\psi X)]^2\sigma_{\rm ib}(\pi^- N) \approx 0.36\,{\rm pb} \ . \tag{16}$$

The corresponding proton-induced cross section, $\sigma^{\psi\psi}_{\rm ib}(pN) \approx 0.51$ pb, is larger. These results are larger than our quoted leading-twist $b\bar{b}$ production cross sections. However, this difference is strongly dependent on the leading-twist parameters. Also, the intrinsic $b\bar{b}$ cross section is proportional to the hN inelastic cross section and changes slowly with $\sqrt{s}$ while the leading-twist cross section has a steep $\sqrt{s}$ dependence, particularly near threshold. Although $b\bar{b}$ production and decay is frame independent, we compare the resulting J/ψ's with the data in the laboratory frame.

There are two ways of producing B mesons from the intrinsic $b\bar{b}$ pairs. The first is by standard fragmentation processes. We will assume that the momentum of the quark lost through fragmentation is small so that a delta function can be used as the fragmentation function, as discussed for leading-twist production. This assumption works well for nonleading D meson production [20,27]. Then the meson and quark distributions are identical. The quark can also coalesce with a projectile valence spectator to produce mesons if the projectile has the corresponding valence quark. The coalescence mechanism introduces flavor correlations between the projectile and the final-state hadrons and produces B's with a larger fraction of the projectile momentum[5]. Such a coalescence model has been used to successfully describe D^-/D^+ production asymmetries [27]. We denote B mesons produced by fragmentation with B_F and those produced by coalescence with B_C. The production processes are illustrated in Fig. 1(e).

If we assume that the b quark fragments into a B meson, the B distribution is

$$\frac{dP_{\rm ib}}{dx_{B_F}} = \int dz \prod_{i=1}^{n} dx_i \frac{dP_{\rm ib}}{dx_1 \ldots dx_n} D_{B/b}(z)\delta(x_{B_F} - zx_b) \ , \tag{17}$$

where n = 4,5 for pion and proton projectiles and $D_{B/b}(z) = \delta(z-1)$ is the b quark fragmentation function. The fragmentation mechanism produces B mesons with 25-30% of the projectile momentum. While this is comparable to or larger than the laboratory fractions carried by B's produced by leading-twist fusion, it is not as large as the result for B_C production. The B_C distribution is

$$\frac{dP_{\rm ib}}{dx_{B_C}} = \int \prod_{i=1}^{n} dx_i \frac{dP_{\rm ib}}{dx_1 \ldots dx_n} \delta(x_{B_C} - x_b - x_1) \ . \tag{18}$$

---

[5]In this model, with a π^- projectile, $B^-(\bar{u}b)$ and $B^0(d\bar{b})$ can be produced by both coalescence and fragmentation while $B^+(u\bar{b})/\overline{B}^0(\bar{d}b)$ can only be produced by fragmentation. In a proton projectile, B^+/B^0 are produced by coalescence and fragmentation. We have not made any assumptions of the relative B meson production rate by coalescence and fragmentation.

In this case, the B_C can carry 40-50 % of the projectile momentum. The increase over B_F production is due to the light valence quark. The B and J/ψ distributions are shown in Fig. 8(c) and 8(d) for the pion and Fig. 9(c) and 9(d) for the proton.

The $\psi\psi$ pairs can be produced either from the decays of the $B\overline{B}$ states produced by fragmentation of the intrinsic $b\bar{b}$ pair, the combination of fragmentation and coalescence, or, from a pion projectile only, double coalescence. The $B_F\overline{B}_F$ distribution is

$$\frac{dP_{\rm ib}}{dx_{B_F\overline{B}_F}} = \int dz_b dz_{\bar{b}} \prod_{i=1}^{n} dx_i \frac{dP_{\rm ib}}{dx_1 \ldots dx_n} D_{B/b}(z_b) D_{\overline{B}/\bar{b}}(z_{\bar{b}}) \delta(x_{B_F} - z_b x_b) \delta(x_{\overline{B}_F} - z_{\bar{b}} x_{\bar{b}}) \ . \tag{19}$$

These $\psi\psi$ pairs have the smallest average momentum fractions of all $\psi\psi$ pairs produced from the intrinsic $|n_V b\bar{b}\rangle$ configuration. If the final-state pair is $B_C\overline{B}_F$,

$$\frac{dP_{\rm ib}}{dx_{B_C\overline{B}_F}} = \int dz \prod_{i=1}^{n} dx_i \frac{dP_{\rm ib}}{dx_1 \ldots dx_n} D_{\overline{B}/\bar{b}}(z) \delta(x_{B_C} - x_b - x_1) \delta(x_{\overline{B}_F} - z x_{\bar{b}}) \ . \tag{20}$$

An initial $|uudb\bar{b}\rangle$ configuration provides no valence antiquark for $\overline{B}_C$ production, thus the $\psi\psi$ pairs resulting from $B_C\overline{B}_F$ decays carry the largest fraction of the proton momentum. However, when the projectile is a pion, such double coalescence is possible. All the pion momentum is transferred to the $B_C\overline{B}_C$ pair

$$\frac{dP_{\rm ib}}{dx_{B_C\overline{B}_C}} = \int \prod_{i=1}^{4} dx_i \frac{dP_{\rm ib}}{dx_1 \ldots dx_4} \delta(x_{B_C} - x_b - x_1) \delta(x_{\overline{B}_C} - x_{\bar{b}} - x_2) \ , \tag{21}$$

i.e. $\langle x_{B_C\overline{B}_C}\rangle \equiv 1$. The $B_C\overline{B}_C \to \psi\psi X$ decay results in high momentum $\psi\psi$ pairs. The $B\overline{B}$ distributions are shown in Figs. 8(a) and 9(a).

The $B\overline{B}$ mass distributions can determine the relative probability for the hadronization mechanism since the available phase space depends on the number of light quarks involved. The mass distribution of the $b\bar{b}$ quark pair is

$$\begin{aligned} \frac{dP_{\rm ib}}{dM^2_{b\bar{b}}} = \int \prod_{i=1}^{n} dx_i d^2k_{T,i} \frac{dx_{b\bar{b}}}{x_{b\bar{b}}} d^2k_{T,b\bar{b}} \frac{dP_{\rm ib}}{\prod_{i=1}^{n} dx_i d^2k_{T,i}} \delta(x_{b\bar{b}} - x_b - x_{\bar{b}}) \\ \times \delta(\vec{k}_{T,b} + \vec{k}_{T,\bar{b}} - \vec{k}_{T,b\bar{b}}) \, \delta\left(\frac{M^2_{T,b\bar{b}}}{x_{b\bar{b}}} - \frac{m^2_{T,b}}{x_b} - \frac{m^2_{T,\bar{b}}}{x_{\bar{b}}}\right) \ . \end{aligned} \tag{22}$$

We find $\langle M_{b\bar{b}}\rangle = 11.75$ GeV. The corresponding $M_{\psi\psi}$ distributions are broad with $\langle M_{\psi\psi}\rangle = 8.0$ GeV. A significant part of the $b\bar{b}$ mass distribution lies below the $B\overline{B}$ production threshold, 10.56 GeV. In order to compute $B_F\overline{B}_F$ production through delta function fragmentation, we restrict $m_{T,b}$ to be larger than m_B. The mass cut reduces the yield by a factor of ~ 20 and increases the average mass to $\langle M_{B_F\overline{B}_F}\rangle = 12.5$ GeV for both projectiles. This is the largest average $B\overline{B}$ mass because although a mass threshold has been imposed, the light quark transverse momentum has not been affected. The average $\psi\psi$ mass is reduced to 7.65 GeV, independent of the projectile.

When $B_C\overline{B}_F$ pairs are created, one of the projectile quarks is included in the heavy meson pair,

$$\begin{aligned} \frac{dP_{\rm ib}}{dM^2_{B_C\overline{B}_F}} = \int \prod_{i=1}^{n} dx_i d^2k_{T,i} \frac{dx_{B_C}}{x_{B_C}} dm^2_{B_C} d^2k_{T,B_C} \frac{dx_{B_C\overline{B}_F}}{x_{B_C\overline{B}_F}} d^2k_{T,B_C\overline{B}_F} \theta(m_{B_F} - 5.28\text{GeV}) \\ \times \frac{dP_{\rm ib}}{\prod_{i=1}^{n} dx_i d^2k_{T,i}} \delta\left(\frac{m^2_{T,B_C}}{x_{B_C}} - \frac{m^2_{T,b}}{x_b} - \frac{m^2_{T,1}}{x_1}\right) \delta(\vec{k}_{T,1} + \vec{k}_{T,b} - \vec{k}_{T,B_C}) \delta(x_{B_C} - x_b - x_1) \\ \times \delta\left(\frac{M^2_{T,B_C\overline{B}_F}}{x_{B_C\overline{B}_F}} - \frac{m^2_{T,B_C}}{x_{B_C}} - \frac{m^2_{T,\overline{B}_F}}{x_{\overline{B}_F}}\right) \delta(\vec{k}_{T,B_C} + \vec{k}_{T,\overline{B}_F} - \vec{k}_{T,B_C\overline{B}_F}) \delta(x_{B_C\overline{B}_F} - x_{B_C} - x_{B_F}) \ , \end{aligned} \tag{23}$$

reducing the invariant mass of the $B\overline{B}$ to 12.2 GeV for pion and 12.4 GeV for proton projectiles. When the projectile is a pion, the $B_C\overline{B}_F$ pair momentum has to be balanced by the remaining valence quark, resulting in a stronger correlation than in a proton with two left over valence quarks and a smaller pair invariant mass. The $\psi\psi$ pair mass is also reduced to 7.5 GeV for a pion projectile and 7.6 GeV for the proton.

The strongest momentum correlations arise from $B_C\overline{B}_C$ production since all the pion momentum is transferred to the meson pair, *i.e.* $x_{B_C\overline{B}_C} \equiv 1$ and $\vec{k}_{T,B_C\overline{B}_C} \equiv 0$. The mass distribution for these pairs can be simplified to

$$\frac{dP_{\rm ib}}{dM^2_{B_C\overline{B}_C}} = \int dx_1 dx_2 \frac{dx_{B_C}}{x_{B_C}(1-x_{B_C})} dm^2_{B_C} dm^2_{\overline{B}_C} d^2k_{T,b} d^2k_{T,\overline{b}} d^2k_{T,\overline{B}_C} \tag{24}$$
$$\times\, \delta\left(\frac{m^2_{T,B_C}}{x_{B_C}} - \frac{m^2_{T,b}}{x_{B_C}-x_1} - \frac{m^2_{T,1}}{x_1}\right) \delta\left(\frac{m^2_{T,\overline{B}_C}}{1-x_{B_C}} - \frac{m^2_{T,\overline{b}}}{1-x_{B_C}-x_2} - \frac{m^2_{T,2}}{x_2}\right)$$
$$\times\, \delta\left(M^2_{T,B_C\overline{B}_C} - \frac{m^2_{T,B_C}}{x_{B_C}} - \frac{m^2_{T,\overline{B}_C}}{1-x_{\overline{B}_C}}\right) \left(m^2_\pi - \frac{m^2_{T,1}}{x_1} - \frac{m^2_{T,2}}{x_2} - \frac{m^2_{T,b}}{x_{B_C}-x_1} - \frac{m^2_{T,\overline{b}}}{1-x_{B_C}-x_2}\right)^{-2} .$$

The x integrations are done in the delta functions, leaving the k_T and B meson mass integrals to balance the pion invariant mass, producing the steepest pair mass distribution with $\langle M_{B_C\overline{B}_C}\rangle = 11.8$ GeV. The $\psi\psi$ mass is also reduced to $\langle M_{\psi\psi}\rangle = 7.05$ GeV. The strong phase space restrictions decrease the relative production probability for this mechanism, making double coalescence rare. However, the detection of such states would be a dramatic proof of the existence of the coalescence mechanism.

With these pair mass distributions, the average $\psi\psi$ momentum is decreased by 5-10% with respect to the average obtained assuming that the b quarks decay to J/ψ. The resulting average momentum fractions and invariant masses are given in Table II.

Although the intrinsic $|n_V b\overline{b}\rangle$ configuration produces fast $\psi\psi$ pairs, with 45-80% of the pion momentum, the $\psi\psi$ production cross section is nearly a factor of 100 too small to account for the NA3 data, primarily due to the small branching ratio for $B \to J/\psi X$ decay.

2. Production From Doubly Intrinsic $Q\overline{Q}$ Configurations

It is possible for configurations with more than one intrinsic heavy quark pair to exist in the projectile, shown in Fig. 1(f). Even though the probability for such configurations is reduced relative to those with only one intrinsic $Q\overline{Q}$, the $\psi\psi$ production cross section could be larger from $|n_V c\overline{c}c\overline{c}\rangle$ or $|n_V c\overline{c}b\overline{b}\rangle$ configurations than the $|n_V b\overline{b}\rangle$ because the square of the B decay branching ratio does not enter. We now discuss $\psi\psi$ production from such configurations.

A. $|n_V c\overline{c}c\overline{c}\rangle$ Configurations

In this section, we follow the arguments of Ref. [9]. The J/ψ production cross section from an $|n_V c\overline{c}\rangle$ configuration is

$$\sigma^\psi_{\rm ic}(hN) = f_{\psi/h}\sigma_{\rm ic}(hN) \ , \tag{25}$$

where $f_{\psi/h}$ is the fraction of the intrinsic $c\overline{c}$ pairs with mass below the $D\overline{D}$ threshold that coalesce into a final-state J/ψ, $c\overline{c} \to J/\psi$. Recently we estimated $f_{\psi/\pi} \approx 0.03$ and $f_{\psi/p} \approx 0.014$ [9] with $m_c = 1.5$ GeV. The predicted cross sections are $\sigma^\psi_{\rm ic}(\pi^- N) = 15$ nb and $\sigma^\psi_{\rm ic}(pN) = 9.8$ nb, in agreement with the NA3 single J/ψ data [28]. Given the intrinsic charm cross section for single J/ψ production, we use the $\psi\psi$ data to estimate the probability to produce two $c\overline{c}$ pairs in the projectile, $P_{\rm icc}$, assuming that all the $\psi\psi$ pair events arise from this mechanism, as in Ref. [9]. Then

$$\sigma^{\psi\psi}_{\rm ic}(hN) = f^2_{\psi/h}\frac{P_{\rm icc}}{P_{\rm ic}}\sigma_{\rm ic}(hN) = f_{\psi/h}\frac{P_{\rm icc}}{P_{\rm ic}}\sigma^\psi_{\rm ic}(hN) \ . \tag{26}$$

The measured value, $\sigma_{\psi\psi} = \sigma^{\psi\psi}_{\rm ic}(\pi^- N) \approx 20$ pb [1], requires $P_{\rm icc} \approx 4.4\% P_{\rm ic}$, implying that it is relatively easy to produce a second intrinsic $Q\overline{Q}$ state if one is already present. If $P_{\rm icc}$ is independent of the projectile identity, $\sigma^{\psi\psi}_{\rm ic}(pN) \approx 6.1$ pb, only 20% of the measured cross section at 400 GeV [2]. Note that if part of the $\pi^- N \to \psi\psi$ production cross section is assumed to arise from leading-twist mechanisms, $P_{\rm icc}$ is reduced.

The single J/ψ distribution in this configuration is

$$\frac{dP_{\rm icc}}{dx_{\psi_1}} = \int \prod_{i=1}^{n} dx_i dx_{\psi_2} \frac{dP_{\rm icc}}{dx_1 \ldots dx_n} \delta(x_{\psi_1} - x_{c_1} - x_{\overline{c}_1})\delta(x_{\psi_2} - x_{c_2} - x_{\overline{c}_2}) \ . \tag{27}$$

We find $\langle x_\psi \rangle = 0.36$ for the pion projectile and $\langle x_\psi \rangle = 0.33$ for the proton. The number of single J/ψ's is twice the number of $\psi\psi$ pairs. The single J/ψ's in the $\psi\psi$ pairs have a lower average momentum fraction than those from $|n_V c\bar{c}\rangle$ Fock states, where $\langle x_\psi \rangle = 0.62$ for a pion and $\langle x_\psi \rangle = 0.51$ for a proton [28,29]. The $\psi\psi$ pair distribution is

$$\frac{dP_{\rm icc}}{dx_{\psi\psi}} = \int dx_{\psi_1} \frac{dP_{\rm icc}}{dx_{\psi_1}} \delta(x_{\psi\psi} - x_{\psi_1} - x_{\psi_2}) \ . \tag{28}$$

Here we find $\langle x_{\psi\psi} \rangle = 0.72$ for the pion and $\langle x_{\psi\psi} \rangle = 0.64$ for the proton. We compare the frame-independent calculation to the combined 150 and 280 GeV data. The $\psi\psi$ pair distributions are in Figs. 10(a) and 11(a) while the single J/ψ distributions are shown in Figs. 10(b) and 11(b).

The $\psi\psi$ pair mass distribution from this configuration is

$$\begin{aligned} \frac{dP_{\rm icc}}{dM^2_{\psi\psi}} = & \int \prod_{i=1}^{n} dx_i d^2k_{T,i} \prod_{j=1}^{2} \frac{dx_{\psi_j}}{x_{\psi_j}} dm^2_{\psi_j} d^2k_{T,\psi_j} \frac{dx_{\psi\psi}}{x_{\psi\psi}} d^2k_{T,\psi\psi} \frac{dP_{\rm icc}}{\prod_{i=1}^{n} dx_i d^2k_{T,i}} \\ & \times \delta\left(\frac{m^2_{T,\psi_j}}{x_{\psi_j}} - \frac{m^2_{T,c_j}}{x_{c_j}} - \frac{m^2_{T,\bar{c}_j}}{x_{\bar{c}_j}} \right) \delta(\vec{k}_{T,c_j} + \vec{k}_{T,\bar{c}_j} - \vec{k}_{T,\psi_j}) \delta(x_{\psi_j} - x_{c_j} - x_{\bar{c}_j}) \\ & \times \delta\left(\frac{M^2_{T,\psi\psi}}{x_{\psi\psi}} - \frac{m^2_{T,\psi_1}}{x_{\psi_1}} - \frac{m^2_{T,\psi_2}}{x_{\psi_2}} \right) \delta(\vec{k}_{T,\psi_1} + \vec{k}_{T,\psi_2} - \vec{k}_{T,\psi\psi}) \delta(x_{\psi\psi} - x_{\psi_1} - x_{\psi_2}) \ , \end{aligned} \tag{29}$$

where $2m_c < m_\psi < 2m_D$. The delta functions insure conservation of momentum for the single J/ψ constituents and the $\psi\psi$ pair. The results are compared with the data in Figs. 10(c) and 11(c). We find $\langle M_{\psi\psi} \rangle \approx 7.7$ GeV for the pion beam and $\langle M_{\psi\psi} \rangle \approx 7.4$ GeV for the proton beam. The smaller $\langle M_{\psi\psi} \rangle$ in pN interactions is compatible with the data [1,2].

This mechanism provides a simple frame-independent source of fast $\psi\psi$ pairs as well as fast single J/ψ's and reproduces the strongly correlated behavior of the $\psi\psi$ pairs. The general agreement with the intrinsic charm model is good.

B. $|n_V c\bar{c}b\bar{b}\rangle$ Configurations

We now discuss $\psi\psi$ production from $|n_V c\bar{c}b\bar{b}\rangle$ configurations. A projectile in such a configuration could produce a $\psi\psi$ pair from a combination of $B \to J/\psi$ decays with $c\bar{c} \to J/\psi$ coalescence. The $\psi\psi$ production cross section is

$$\sigma^{\psi\psi}_{\rm icb}(hN) = f_{\psi/h} \frac{P_{\rm icb}}{P_{\rm ib}} \sigma_{\rm ib}(hN) BR(B \to J/\psi X) \ . \tag{30}$$

If we assume $P_{\rm icb}/P_{\rm ib} \approx P_{\rm icc}/P_{\rm ic}$, then $\sigma^{\psi\psi}_{\rm icb}(\pi^- N) \approx 0.044$ pb and $\sigma^{\psi\psi}_{\rm icb}(pN) \approx 0.020$ pb. These cross sections are equivalent to those from leading-twist $b\bar{b}$ production, much less than the measured cross sections. The πN cross section is larger since $f_{\psi/p} < f_{\psi/\pi}$.

The J/ψ distribution from this state is

$$\frac{dP_{\rm icb}}{dx_\psi} = \int \prod_{i=1}^{n} dx_i \frac{dP_{\rm icb}}{dx_1 \ldots dx_n} \delta(x_\psi - x_c - x_{\bar{c}}) \tag{31}$$

since the intrinsic $c\bar{c}$ coalescence is unaffected by the b quark hadronization. We find $\langle x_\psi \rangle = 0.31$ from a pion projectile and $\langle x_\psi \rangle = 0.28$ from a proton, independent of frame. These J/ψ distributions are shown in the dot-dashed curves in Fig. 12(a) and 13(a).

If the B meson is produced by fragmentation,

$$\frac{dP_{\rm icb}}{dx_{B_F}} = \int dz \prod_{i=1}^{n} dx_i \frac{dP_{\rm icb}}{dx_1 \ldots dx_n} dx_\psi \delta(x_\psi - x_c - x_{\bar{c}}) D_{B/b}(z) \delta(x_{B_F} - z x_b) \ . \tag{32}$$

Alternatively, if the b quark hadronizes by coalescence,

$$\frac{dP_{\rm icb}}{dx_{B_C}} = \int \prod_{i=1}^{n} dx_i \frac{dP_{\rm icb}}{dx_1 \ldots dx_n} dx_\psi \delta(x_\psi - x_c - x_{\bar{c}}) \delta(x_{B_C} - x_b - x_1) \ . \tag{33}$$

Again, note that the B production is frame independent but the J/ψ distributions are presented in the laboratory frame. The B_F and B_C distributions are given in Figs. 12(a) and 13(a) for the pion and proton while the J/ψ distributions from the decays appear in Figs. 12(b) and 13(b).

The $\psi\psi$ pairs from the $|n_V c\bar{c}b\bar{b}\rangle$ Fock state arise from a $B \to J/\psi X$ decay combined with $c\bar{c} \to J/\psi$ coalescence and boosted to the laboratory frame. The average $\psi\psi$ momentum is larger when the parent B was produced by coalescence. The results are shown in Figs. 12(c) and 13(c). The average momentum fractions of the B mesons and the $\psi\psi$ pairs from this configuration are given in Table III. While the average longitudinal momentum fraction is relatively large, the pair mass is sharply peaked near threshold with $\langle M_{\psi\psi}\rangle \approx 6.5$ GeV, as shown in Figs. 12(d) and 13(d). Additionally, the cross section is a factor of 500 below the data. Therefore it is unlikely that this mechanism could produce the $\psi\psi$ pairs observed by NA3.

3. Leading-Twist J/ψ Production with an Intrinsic Charm Configuration

We have also studied the possibility of double J/ψ production by simultaneous leading-twist fusion and coalescence of an intrinsic $c\bar{c}$ pair, $c\bar{c} \to J/\psi$. In this case, the parton distributions of the projectile pion and proton are obtained from the $|nc\bar{c}\rangle$ Fock configurations, as shown in Fig. 1(g), where n represents the valence quarks plus other light partons. Thus for $q\bar{q}$ annihilation with a pion valence quark, only the lowest intrinsic charm Fock state, $|\bar{u}dc\bar{c}\rangle$, is needed. For gluon fusion, an additional gluon is necessary, $|\bar{u}dgc\bar{c}\rangle$. Annihilation with a sea quark requires at least a six particle Fock state, $|\bar{u}dq\bar{q}c\bar{c}\rangle$. With a proton projectile, the lowest-lying configurations have five, six, and seven partons. The valence quark probability distribution from an intrinsic $c\bar{c} \to J/\psi$ state is given by

$$q_{v_\pi}(x_1) = \frac{dP_{\rm ic}}{dx_1} = \int dx_{2p} dx_c dx_{\bar{c}} dx_{\psi_2} \frac{dP_{\rm ic}}{dx_1 \ldots dx_n} \delta(x_{\psi_2} - x_c - x_{\bar{c}}) \ , \tag{34}$$

where x_{2p} is a light quark in the projectile (the $2p$ subscript is used to distinguish it from the target momentum fraction) and x_1 is the projectile parton contributing to the fusion process, either a valence or sea quark or a gluon. We also need the ψ_2 distribution when x_1 is fixed by the fusion process,

$$q_{v_\pi}(x_1; x_{\psi_2}) = \frac{dP_{\rm ic}}{dx_1 dx_{\psi_2}}|_{x_1} = \int dx_{2p} dx_c dx_{\bar{c}} \frac{dP_{\rm ic}}{dx_1 \ldots dx_n} \delta(x_{\psi_2} - x_c - x_{\bar{c}}) \ . \tag{35}$$

The sea quark and gluon distributions are similarly calculated. The target parton distribution functions are GRV LO [10] and Duke-Owens 1.1 [12]. The projectile and target momentum fractions in the leading-twist fusion process are $x_{1,2} = (\pm x_{\psi_1} + \sqrt{x_{\psi_1}^2 + 4\tau^2})/2$, where $2m_c/\sqrt{s} < \tau < 2m_D/\sqrt{s}$. The $c\bar{c}$ pair is assumed to neutralize its color and produce a J/ψ by emitting a soft gluon without significant momentum loss.

The J/ψ produced by parton fusion has the momentum distribution

$$\frac{d\sigma}{dx_{\psi_1}} = 2F f_{\psi/h} \int_{2m_c/\sqrt{s}}^{2m_D/\sqrt{s}} \frac{\tau d\tau}{x_2\sqrt{x_{\psi_1}^2 + 4\tau^2}} [q_{v_p}(x_2) q_{v_\pi}(x_1) \hat{\sigma}_{q\bar{q}\to c\bar{c}} + G_p(x_2) G_\pi(x_1) \hat{\sigma}_{gg\to c\bar{c}}$$
$$+ q_{s_p}(x_2) q_{s_\pi}(x_1) \hat{\sigma}_{q\bar{q}\to c\bar{c}}] \ , \tag{36}$$

written in order of increasing number of partons in the minimal projectile Fock state. We define $xq_{v_p}(x) = xu_p(x) + x\bar{d}_p(x)$ for annihilation with the $\pi^-(\bar{u}d)$ valence quarks and $xq_{s_p}(x) = xu_p(x) + x\bar{u}_p(x) + xd_p(x) + x\bar{d}_p(x) + 2xs_p(x)$ for $q\bar{q}$ annihilation with pion sea quarks where $xu_p = xu_{v_p} + xu_{s_p}$ and $xd_p = xd_{v_p} + xd_{s_p}$. These J/ψ distributions, shown in Figs. 14(a) and 15(a) for pion and proton beams, are central. In the laboratory frame, $\langle x_\psi\rangle_{\rm pf} \approx 0.26$ from $\pi^- p$ interactions and $\langle x_\psi\rangle_{\rm pf} \approx 0.18$ from pp interactions, nearly independent of the beam energy. The J/ψ distribution from the intrinsic charm state is

$$\frac{d\sigma}{dx_{\psi_2}} = 2F f_{\psi/h} \int_0^1 dx_{\psi_1} \int_{2m_c/\sqrt{s}}^{2m_D/\sqrt{s}} \frac{\tau d\tau}{x_2\sqrt{x_{\psi_1}^2 + 4\tau^2}} [q_{v_p}(x_2) q_{v_\pi}(x_1; x_{\psi_2}) \hat{\sigma}_{q\bar{q}\to c\bar{c}}$$
$$+ G_p(x_2) G_\pi(x_1; x_{\psi_2}) \hat{\sigma}_{gg\to c\bar{c}} + q_{s_p}(x_2) q_{s_\pi}(x_1; x_{\psi_2}) \hat{\sigma}_{q\bar{q}\to c\bar{c}}] \ . \tag{37}$$

These distributions, shown in the laboratory frame in Figs. 14(b) and 15(b), have larger average momentum fractions, $\langle x_\psi\rangle_{\rm ic} \approx 0.56$ and 0.46 for pion and proton projectiles. Thus one fast and one slow J/ψ are produced, in agreement with the single J/ψ data. The $\psi\psi$ distributions are strongly forward peaked, with $\langle x_{\psi\psi}\rangle \approx 0.84$ for a pion and, for a

proton, $\langle x_{\psi\psi} \rangle \approx 0.68$, larger than the data. The average $\psi\psi$ pair mass is ≈ 8 GeV. However, the mass distributions do not appear strongly correlated.

The parameter F is introduced since the leading-twist fusion cross section includes all $c\bar{c}$ resonances below the $D\overline{D}$ threshold. When $m_c = 1.5$, $F \approx 1/5$. We also include the factor $f_{\psi/h}$ for J/ψ production from the intrinsic charm state. These two suppression factors predict a $\psi\psi$ production cross section of ≈ 3.5 pb for πp and ≈ 2.5 pb for pp production.

IV. Summary

A summary of all the predicted cross sections is given in Table IV. From the magnitude of the calculated cross sections alone, it appears that approximately 50% of the measured $\psi\psi$ cross section can be attributed to the leading-twist mechanisms. However, only the higher-twist mechanisms produce fast $\psi\psi$ pairs. The intrinsic heavy quark states offer a promising alternative, especially since all $\psi\psi$ pairs produced through these mechanisms carry a significant fraction of the projectile momentum. Particularly, the $|n_V c\bar{c}c\bar{c}\rangle$ configuration can also account for the size of the $\psi\psi$ cross section, as discussed in [9].

The correlations in $B\overline{B}$ production also suggest an intriguing test of the intrinsic heavy quark mechanism. In particular, if both B's are produced by coalescence, all the pion momentum would be transferred to the $B\overline{B}$ pair. The same type of correlation should be observable in $D\overline{D}$ production in πA interactions. Measurements of the D^-/D^+ asymmetry could be extended to the momentum and invariant mass distributions of $D\overline{D}$ pairs.

We thank S.J. Brodsky, P. Hoyer, G. Ingelman, and W.-K. Tang for stimulating discussions and J.-C. Peng for encouragement and for providing the B decay Monte Carlo.

[1] J. Badier *et al.*, Phys. Lett. **114B** (1982) 457.
[2] J. Badier *et al.*, Phys. Lett. **158B** (1985) 85.
[3] R.E. Ecclestone and D.M. Scott, Phys. Lett. **120B** (1983) 237.
[4] B. Humpert and P. Mery, Phys. Lett. **124B** (1983) 265.
[5] V.G. Kartvelishvili and Sh.M. Ésakiya, Sov. J. Nucl. Phys. **38**(3) (1983) 430 [Yad. Fiz. **38** (1983) 722].
[6] V. Barger, F. Halzen, and W.Y. Keung, Phys. Lett. **119B** (1982) 453.
[7] B.-A. Li and K.-F. Liu, Phys. Rev. **D29** (1984) 426.
[8] S.J. Brodsky, P. Hoyer, C. Peterson, and N. Sakai, Phys. Lett. **B93** (1980) 451; S.J. Brodsky, C. Peterson and N. Sakai, Phys. Rev. **D23** (1981) 2745.
[9] R. Vogt and S.J. Brodsky, LBL-36754, SLAC-PUB-95-6753, submitted to Phys. Lett. **B**.
[10] M. Gluck, E. Reya, and A. Vogt, Z. Phys. **C53** (1992) 127;
[11] M. Gluck, E. Reya, and A. Vogt, Z. Phys. **C53** (1992) 651.
[12] J.F. Owens, Phys. Lett. **B266** (1991) 126.
[13] J.F. Owens, Phys. Rev. **D30** (1984) 943.
[14] P. Nason, S. Dawson, and R.K. Ellis, Nucl. Phys. **B327** (1989) 49.
[15] R. Baier and R. Rückl, Z. Phys. **C19** (1983) 251.
[16] G. Schuler, CERN preprint CERN-TH.7170/94, submitted to Phys. Rep.
[17] R.K. Ellis, in *Physics at the 100 GeV Scale*, Proceedings of the 17th SLAC Summer Institute, Stanford, California, 1989, edited by E.C. Brennan (SLAC Report No. 361, Stanford, 1990).
[18] M. Aguilar-Benitez, Particle Data Group, Phys. Rev. **D50** (1994) 1173.
[19] C. Peterson, D. Schlatter, I. Schmitt, and P. Zerwas, Phys. Rev. **D27** (1983) 105.
[20] R. Vogt, S.J. Brodsky, and P. Hoyer, Nucl. Phys. **B383** (1992) 643.
[21] J. Chrin, in *Proc. Int. Symp. on Production and Decay of Heavy Flavors*, Stanford, California, 1987, edited by E. Bloom and A. Fridman, p. 131.
[22] R. Balest *et al.*, CLEO Coll., CLNS-94-1315.
[23] S.J. Brodsky, P. Hoyer, A.H. Mueller, and W.-K. Tang, Nucl. Phys. **B369** (1992) 519.
[24] P. Hoyer and S.J. Brodsky, Nashville Part. Prod. 1990, p. 238.
[25] J.J. Aubert *et al.*, Phys. Lett. **110B** (1982) 73; E. Hoffmann and R. Moore, Z. Phys. **C20** (1983) 71.
[26] M. Adamovich *et al.*, Phys. Lett. **B305** (1993) 402; G.A. Alves *et al.*, Phys. Rev. Lett. **72** (1994) 812.
[27] R. Vogt and S.J. Brodsky, LBL-35380, SLAC-PUB-6468, Nucl. Phys. **B**, in press.
[28] J. Badier *et al.*, Z. Phys. **C20** (1983) 101.
[29] R. Vogt, S.J. Brodsky, and P. Hoyer, Nucl. Phys. **B360** (1991) 67.

Figure Captions

Figure 1. (a) Examples of $\mathcal{O}(\alpha_s^4)$ QCD graphs for $gg \to \psi\psi$. (b) The diagrams for $\mathcal{O}(\alpha_s^4)$ $q\overline{q} \to \psi\psi$ production. (c) Leading-twist $b\overline{b}$ production by $q\overline{q}$ annihilation and gg fusion. (d) Drell-Yan type resonance production. The intermediate state contains four quarks and $\underline{\psi}$ denotes a color-octet-vector $c\overline{c}$. (e) An intrinsic $b\overline{b}$ pair illustrating the coalescence (B_C) and fragmentation (B_F) production processes. (f) An example of a pair of intrinsic $Q\overline{Q}$ states in the projectile. (g) Diagrams of leading-twist J/ψ production with the projectile in an intrinsic $c\overline{c}$ state. Fusion production by valence quark annihilation, gluon fusion, and sea quark annihilation are shown respectively.

Figure 2. The $\mathcal{O}(\alpha_s^4)$ $\pi^- p \to \psi\psi$ distributions in the laboratory frame compared to the NA3 data. The $x_{\psi\psi}$ distributions are shown in (a), the x_ψ distributions in (b), and the pair mass distribution in (c). The curves show: at 150 GeV, GRV LO (solid) and DO 1.1 (dashed); at 280 GeV, GRV LO (dot-dashed) and DO 1.1 (dotted).

Figure 3. The $\mathcal{O}(\alpha_s^4)$ $pp \to \psi\psi$ distributions in the laboratory frame. The $x_{\psi\psi}$ distributions are shown in (a), the x_ψ distributions in (b), and the pair mass distribution is compared to the NA3 data in (c). The curves show: at 400 GeV, GRV LO (solid) and DO 1.1 (dashed); at 800 GeV, GRV LO (dot-dashed) and DO 1.1 (dotted).

Figure 4. Leading-twist $\pi^- p \to b\overline{b}$ production in the laboratory frame, compared to the NA3 $\psi\psi$ data. The $x_{b\overline{b}}$ distributions are shown in (a) and the x_b distributions in (c) with GRV LO (solid) and DO 1.1 (dashed) at 150 GeV and GRV LO (dot-dashed) and DO 1.1 (dotted) at 280 GeV. The remaining results, with the GRV set, compares the assumptions of $b\overline{b}$ decay vs. $B\overline{B}$ production and decay. The solid and dot-dashed curves give the $b\overline{b}$ distributions at 150 and 280 GeV while the dashed and dotted curves show the $B\overline{B}$ distributions at the same energies. The $x_{\psi\psi}$ and x_ψ distributions are shown in (b) and (d), the $\psi\psi$ pair mass distribution in (f), and the invariant mass of the $b\overline{b}$ and $B\overline{B}$ pairs in (e).

Figure 5. Leading-twist $pp \to b\overline{b}$ production in laboratory frame. The $x_{b\overline{b}}$ distributions are shown in (a), the x_b distributions in (c) with GRV LO (solid) and DO 1.1 (dashed) at 400 GeV and GRV LO (dot-dashed) and DO 1.1 (dotted) at 800 GeV. The remaining results, with the GRV set, compares the assumptions of $b\overline{b}$ decay vs. $B\overline{B}$ production and decay. The solid and dot-dashed curves give the $b\overline{b}$ distributions at 400 and 800 GeV while the dashed and dotted curves show the $B\overline{B}$ distributions at the same energies. The $x_{\psi\psi}$ and x_ψ distributions are shown in (b) and (d), the $\psi\psi$ pair mass distribution in (f), compared to the NA3 data, and the invariant mass of the $b\overline{b}$ and $B\overline{B}$ pairs in (e).

Figure 6. The $\pi^- N \to 2^{++} c\overline{c}c\overline{c} \to \psi\psi$ distributions in the laboratory frame, compared to the NA3 data. The $x_{\psi\psi}$ distributions are shown in (a), the x_ψ distributions in (b), and the $M_{\psi\psi}$ distribution in (c). The calculations are: at 150 GeV, GRV LO (solid) and scaling (dashed) gluon distributions; at 280 GeV, GRV LO (dot-dashed) and scaling (dotted) gluons.

Figure 7. The $pN \to 2^{++} c\overline{c}c\overline{c} \to \psi\psi$ distributions in the laboratory frame. The $x_{\psi\psi}$ distributions are shown in (a), the x_ψ distributions in (b), and the $M_{\psi\psi}$ distribution is compared with the NA3 data in (c). The calculations are: at 400 GeV, GRV LO (solid) and scaling (dashed) gluon distributions; at 800 GeV, GRV LO (dot-dashed) and scaling (dotted) gluons.

Figure 8. Frame-independent $b\overline{b}$ production is calculated from an intrinsic $|\overline{u}db\overline{b}\rangle$ configuration. In (a), the $x_{B_F\overline{B}_C}$ (solid) and $x_{B_F\overline{B}_F}$ (dashed) distributions are shown. If both B's are produced by coalescence, $x_{B_C\overline{B}_C} \equiv 1$. In (c), the x_{B_F} (solid) and x_{B_C} (dashed) distributions are shown. The invariant masses of the $b\overline{b}$ (solid), $B_F\overline{B}_F$ (dashed), $B_C\overline{B}_F$ (dot-dashed), and $B_C\overline{B}_C$ (dotted) pairs are shown in (e). The J/ψ distributions are in the laboratory frame. The $x_{\psi\psi}$ distributions are shown in (b). The solid and dot-dashed curves show $B_F\overline{B}_C \to \psi\psi$ pairs at 150 and 280 GeV while the dashed and dotted curves show $B_F\overline{B}_F \to \psi\psi$ pairs at 150 and 280 GeV. The thin solid and dashed curves are results from $B_C\overline{B}_C \to \psi\psi$ decays at 150 and 280 GeV. The x_ψ distributions are in (d). The $B_C \to J/\psi X$ decays are given in the dashed (150 GeV) and dot-dashed (280 GeV) while $B_F \to J/\psi X$ decays are shown in the solid (150 GeV) and dotted (280 GeV) curves. Finally, the $M_{\psi\psi}$ distributions from $B_F\overline{B}_F$ decays (solid) and $B_C\overline{B}_C$ decays (dashed) are given in (f).

Figure 9. Frame-independent $b\bar{b}$ production is calculated from an intrinsic $|uudb\bar{b}\rangle$ configuration. In (a), the $x_{B_F\overline{B}_C}$ (solid) and $x_{B_F\overline{B}_F}$ (dashed) distributions are shown. In (c), the x_{B_F} (solid) and x_{B_C} (dashed) distributions are shown. The invariant masses of the $b\bar{b}$ (solid), $B_F\overline{B}_F$ (dashed), and $B_C\overline{B}_F$ (dot-dashed) pairs are shown in (e). The J/ψ results are shown in the laboratory frame. The $x_{\psi\psi}$ distributions are shown in (b). The solid and dot-dashed curves show the $B_F\overline{B}_C \to \psi\psi$ pairs at 400 and 800 GeV while the dashed and dotted curves show $B_F\overline{B}_F \to \psi\psi$ decays at 400 and 800 GeV. The x_ψ distributions are in (d). The $B_C \to J/\psi X$ decays are given in the dashed (400 GeV) and dot-dashed (800 GeV) and the $B_F \to J/\psi X$ decays are given by the solid (400 GeV) and dotted (800 GeV) curves. Finally, the $M_{\psi\psi}$ distribution is in (f).

Figure 10. Frame-independent $\psi\psi$ production from a $|\bar{u}dc\bar{c}c\bar{c}\rangle$ configuration. The $x_{\psi\psi}$ distribution is shown in (a), the x_ψ distribution in (b), and the mass distribution in (c).

Figure 11. Frame-independent $\psi\psi$ production from a $|uudc\bar{c}c\bar{c}\rangle$ configuration. The $x_{\psi\psi}$ distribution is shown in (a), the x_ψ distribution in (b), and the mass distribution in (c).

Figure 12. Results for J/ψ and $\psi\psi$ production from an intrinsic $|\bar{u}dc\bar{c}b\bar{b}\rangle$ configuration. In (a) we show the frame-independent results for: $c\bar{c} \to J/\psi$ (solid), B_C (dashed) and B_F (dot dashed) production. All other results are in the laboratory frame. In (b), the B_C decays are given by the solid and dotted curves for 150 and 280 GeV while the B_F decays are shown in the dashed and dot-dashed curves for 150 and 280 GeV. In (c) and (d) the $x_{\psi\psi}$ and $M_{\psi\psi}$ distributions result from the combination of $c\bar{c} \to J/\psi$ with a decaying B: pairing with a B_C results in the dashed (150 GeV) and dotted (280 GeV) curves while a B_F pairing produces the results given in the solid (150 GeV) and dot-dashed (280 GeV) curves.

Figure 13. Results for J/ψ and $\psi\psi$ production from an intrinsic $|uudc\bar{c}b\bar{b}\rangle$ configuration. In (a) we show the frame-independent results for: $c\bar{c} \to J/\psi$ (solid), B_C (dashed) and B_F (dot dashed) production. All other results are in the laboratory frame. In (b), the B_C decays are given by the solid and dotted curves for 150 and 280 GeV while the B_F decays are shown in the dashed and dot-dashed curves for 150 and 280 GeV. In (c) and (d) the $x_{\psi\psi}$ and $M_{\psi\psi}$ distributions result from the combination of $c\bar{c} \to J/\psi$ with a decaying B: pairing with a B_C results in the dashed (150 GeV) and dotted (280 GeV) curves while a B_F pairing produces the results given in the solid (150 GeV) and dot-dashed (280 GeV) curves.

Figure 14. $\psi\psi$ pairs produced by simultaneous J/ψ production by leading-twist fusion with a pion in an $|\bar{u}dnc\bar{c}\rangle$ configuration, in the laboratory frame. The leading-twist and intrinsic $c\bar{c}$ J/ψ distributions are given in (a) and (b), and the $x_{\psi\psi}$ and mass distributions are shown in (c) and (d). The calculations are: at 150 GeV, GRV LO (solid) and DO 1.1 (dashed); at 280 GeV, GRV LO (dot-dashed) and DO 1.1 (dotted).

Figure 15. $\psi\psi$ pairs produced by simultaneous J/ψ production by leading-twist fusion with a proton in an $|uudnc\bar{c}\rangle$ configuration, in the laboratory frame. The leading-twist and intrinsic $c\bar{c}$ J/ψ distributions are given in (a) and (b), and the $x_{\psi\psi}$ and mass distributions are shown in (c) and (d). The calculations are: at 400 GeV, GRV LO (solid) and DO 1.1 (dashed); at 800 GeV, GRV LO (dot-dashed) and DO 1.1 (dotted).

TABLE I. The average laboratory momentum fractions and invariant masses for leading-twist $B\overline{B}$ production and decay in hp interactions calculated with the GRV LO parton distributions. Note that the combined $\pi^- N \to \psi\psi X$ data give $\langle x_\psi \rangle = 0.33$, $\langle x_{\psi\psi} \rangle = 0.66$, and $\langle M_{\psi\psi} \rangle = 7.4$ GeV while the average $\psi\psi$ mass from the $pN \to \psi\psi X$ measurements is $\langle M_{\psi\psi} \rangle = 6.8$ GeV.

h, $p_{\rm beam}$ (GeV)	$\langle x_B \rangle$	$\langle x_\psi \rangle$	$\langle x_{B\overline{B}} \rangle$	$\langle x_{\psi\psi} \rangle$	$\langle M_{B\overline{B}} \rangle$ (GeV)	$\langle M_{\psi\psi} \rangle$ (GeV)
π^-, 150	0.34	0.24	0.65	0.50	11.5	7.1
π^-, 280	0.27	0.19	0.52	0.41	12.1	7.4
p, 400	0.19	0.13	0.37	0.29	11.9	7.3
p, 800	0.15	0.10	0.27	0.22	12.3	7.5

TABLE II. The average momentum fractions of B and $B\overline{B}$ production and decay from intrinsic $|n_V b\bar{b}\rangle$ states in the projectile h. The B results are frame independent, the J/ψ and $\psi\psi$ averages are in the laboratory frame. The invariant masses are given in GeV. Recall that B_F denotes B mesons produced by fragmentation while B_C denotes mesons produced by coalescence with projectile valence quarks. Note that the combined $\pi^- N \to \psi\psi X$ data give $\langle x_\psi \rangle = 0.33$, $\langle x_{\psi\psi} \rangle = 0.66$, and $\langle M_{\psi\psi} \rangle = 7.4$ GeV while the average $\psi\psi$ mass from the $pN \to \psi\psi X$ measurements is $\langle M_{\psi\psi} \rangle = 6.8$ GeV.

	B_F		B_C		$B_F\overline{B}_F$		$B_F\overline{B}_C$		$B_C\overline{B}_C$	
h, $p_{\rm beam}$ (GeV)	$\langle x_B \rangle$	$\langle x_\psi \rangle$	$\langle x_B \rangle$	$\langle x_\psi \rangle$	$\langle x_{B\overline{B}} \rangle$	$\langle x_{\psi\psi} \rangle$	$\langle x_{B\overline{B}} \rangle$	$\langle x_{\psi\psi} \rangle$	$\langle x_{B\overline{B}} \rangle$	$\langle x_{\psi\psi} \rangle$
π^-, 150	0.33	0.35	0.50	0.44	0.64	0.71	0.80	0.76	1.0	0.81
π^-, 280	0.33	0.31	0.50	0.40	0.64	0.60	0.80	0.67	1.0	0.75
p, 400	0.29	0.26	0.43	0.35	0.55	0.51	0.69	0.58		
p, 800	0.29	0.24	0.43	0.32	0.55	0.44	0.69	0.52		
					$\langle M_{B\overline{B}} \rangle$	$\langle M_{\psi\psi} \rangle$	$\langle M_{B\overline{B}} \rangle$	$\langle M_{\psi\psi} \rangle$	$\langle M_{B\overline{B}} \rangle$	$\langle M_{\psi\psi} \rangle$
π^-					12.5	7.65	12.2	7.5	11.8	7.05
p					12.5	7.65	12.4	7.6		

TABLE III. The average momentum fractions for B production and decay from an intrinsic $c\bar{c}b\bar{b}$ state. The $\psi\psi$ pairs are produced through $c\bar{c} \to J/\psi$ coalescence and $B \to J/\psi X$ decay. The B averages are frame independent, the J/ψ and $\psi\psi$ averages are in the laboratory frame. Recall that B_F denotes B mesons produced by fragmentation while B_C denotes mesons produced by coalescence with projectile valence quarks. Note that the combined $\pi^- N \to \psi\psi X$ data give $\langle x_\psi \rangle = 0.33$, $\langle x_{\psi\psi} \rangle = 0.66$.

	B_F		B_C		ψB_F	ψB_C
h, $p_{\rm beam}$ (GeV)	$\langle x_B \rangle$	$\langle x_\psi \rangle$	$\langle x_B \rangle$	$\langle x_\psi \rangle$	$\langle x_{\psi\psi} \rangle$	$\langle x_{\psi\psi} \rangle$
π^-, 150	0.23	0.30	0.35	0.36	0.69	0.74
π^-, 280	0.23	0.25	0.35	0.32	0.62	0.67
p, 400	0.21	0.22	0.32	0.28	0.54	0.60
p, 800	0.21	0.19	0.32	0.25	0.49	0.56

TABLE IV. A summary of $\sigma_{\psi\psi}$ for all the studied processes. When only one value is given for more than one energy, the results are nearly energy independent.

Process	$\sigma_{\psi\psi}(\pi^- N)$ (pb)		$\sigma_{\psi\psi}(pN)$ (pb)	
	150 GeV	280 GeV	400 GeV	800 GeV
NA3	18 ± 8	30 ± 10	27 ± 10	
$\mathcal{O}(\alpha_s^4)$	7.4	16.5	7.2	26.0
$\mathcal{O}(\alpha_s^2)$ $b\bar{b}$	0.028	0.24	0.03	0.16
2^{++} $c\bar{c}c\bar{c}$	1.7	10.0	12.8	55.2
$\|n_V b\bar{b}\rangle$		0.36		0.51
$\|n_V c\bar{c}c\bar{c}\rangle$		$\equiv 20$		6.1
$\|n_V c\bar{c}b\bar{b}\rangle$		0.044		0.020
$\|nc\bar{c}\rangle$	3.3	4.3	1.9	2.8

Figure 2

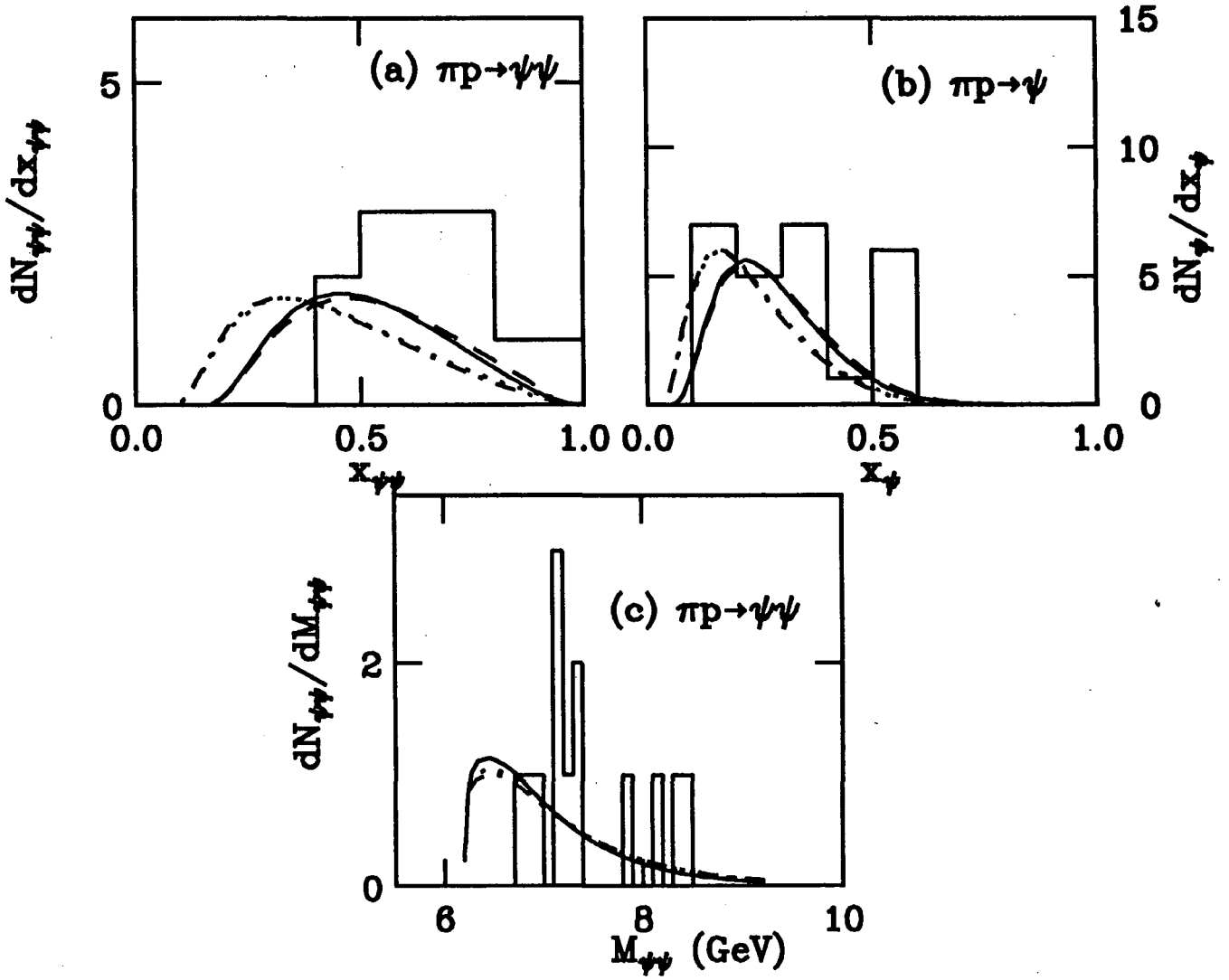
(a) πp→ψψ
(b) πp→ψ
(c) πp→ψψ
dN_ψψ/dx_ψψ
dN_ψ/dx_ψ
dN_ψψ/dM_ψψ
x_ψψ
x_ψ
M_ψψ (GeV)
0.0
0.5
1.0
0
5
10
15
2
6
8
10

Figure 3

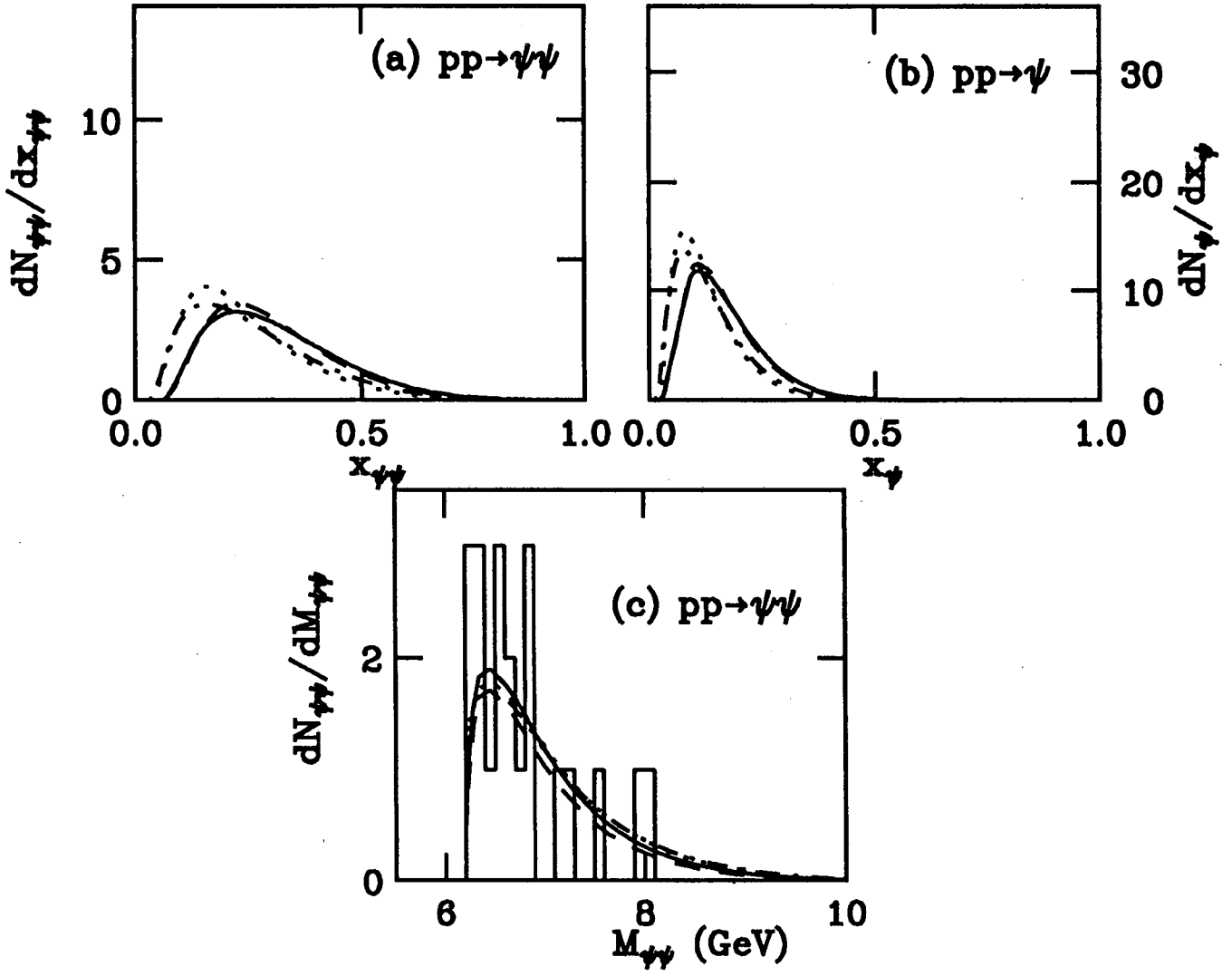
(a) pp→ψψ
(b) pp→ψ
(c) pp→ψψ
dN_ψψ/dx_ψψ
dN_ψ/dx_ψ
dN_ψψ/dM_ψψ
x_ψψ
x_ψ
M_ψψ (GeV)
0.0
0.5
1.0
0
5
10
20
30
2
6
8

Figure 4

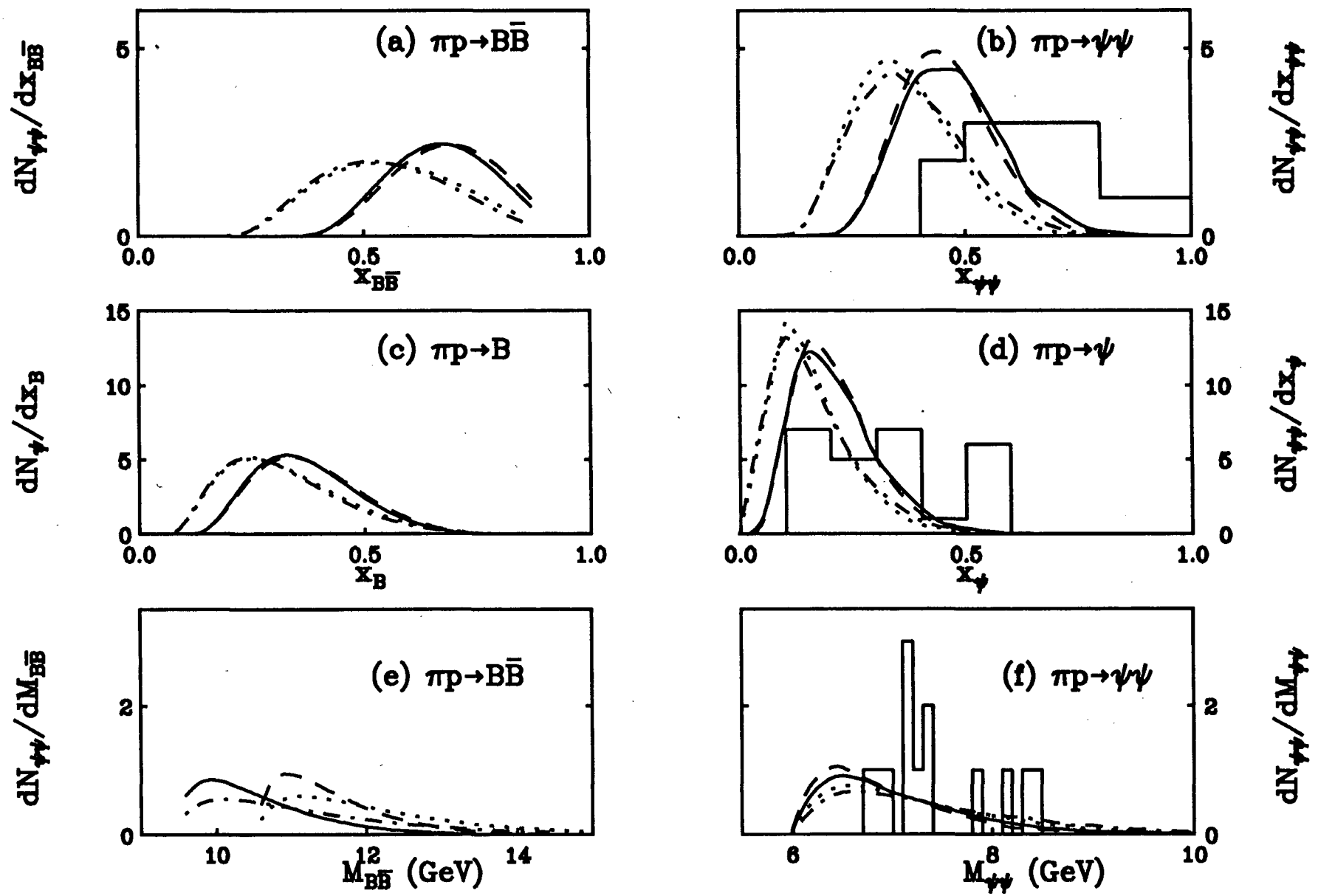
(a) πp→BB̄
(b) πp→ψψ
(c) πp→B
(d) πp→ψ
(e) πp→BB̄
(f) πp→ψψ
dN_ψψ/dx_BB̄
dN_ψψ/dx_ψψ
dN_ψ/dx_B
dN_ψψ/dx_ψ
dN_ψψ/dM_BB̄
dN_ψψ/dM_ψψ
x_BB̄
x_ψψ
x_B
x_ψ
M_BB̄ (GeV)
M_ψψ (GeV)
0.0
0.5
1.0
0
5
10
15
2
6
8
10
12
14

Figure 5

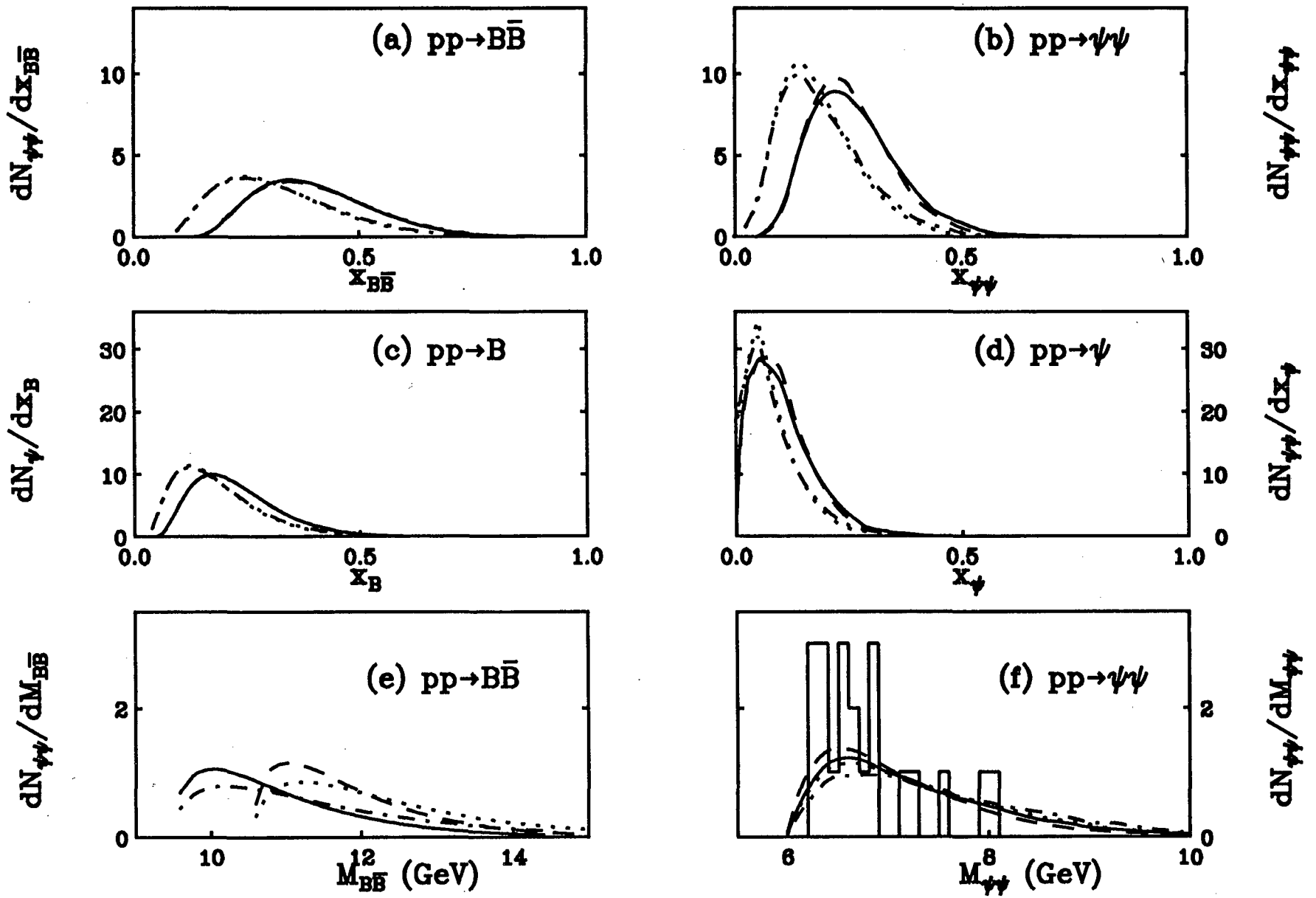
(a) pp→BB̄
(b) pp→ψψ
(c) pp→B
(d) pp→ψ
(e) pp→BB̄
(f) pp→ψψ
dN_ψψ/dx_BB̄
dN_ψψ/dx_ψψ
dN_ψ/dx_B
dN_ψψ/dx_ψ
dN_ψψ/dM_BB̄
dN_ψψ/dM_ψψ
x_BB̄
x_ψψ
x_B
x_ψ
M_BB̄ (GeV)
M_ψψ (GeV)
0.0
0.5
1.0
0
5
10
20
30
2
6
8
10
12
14

Figure 6

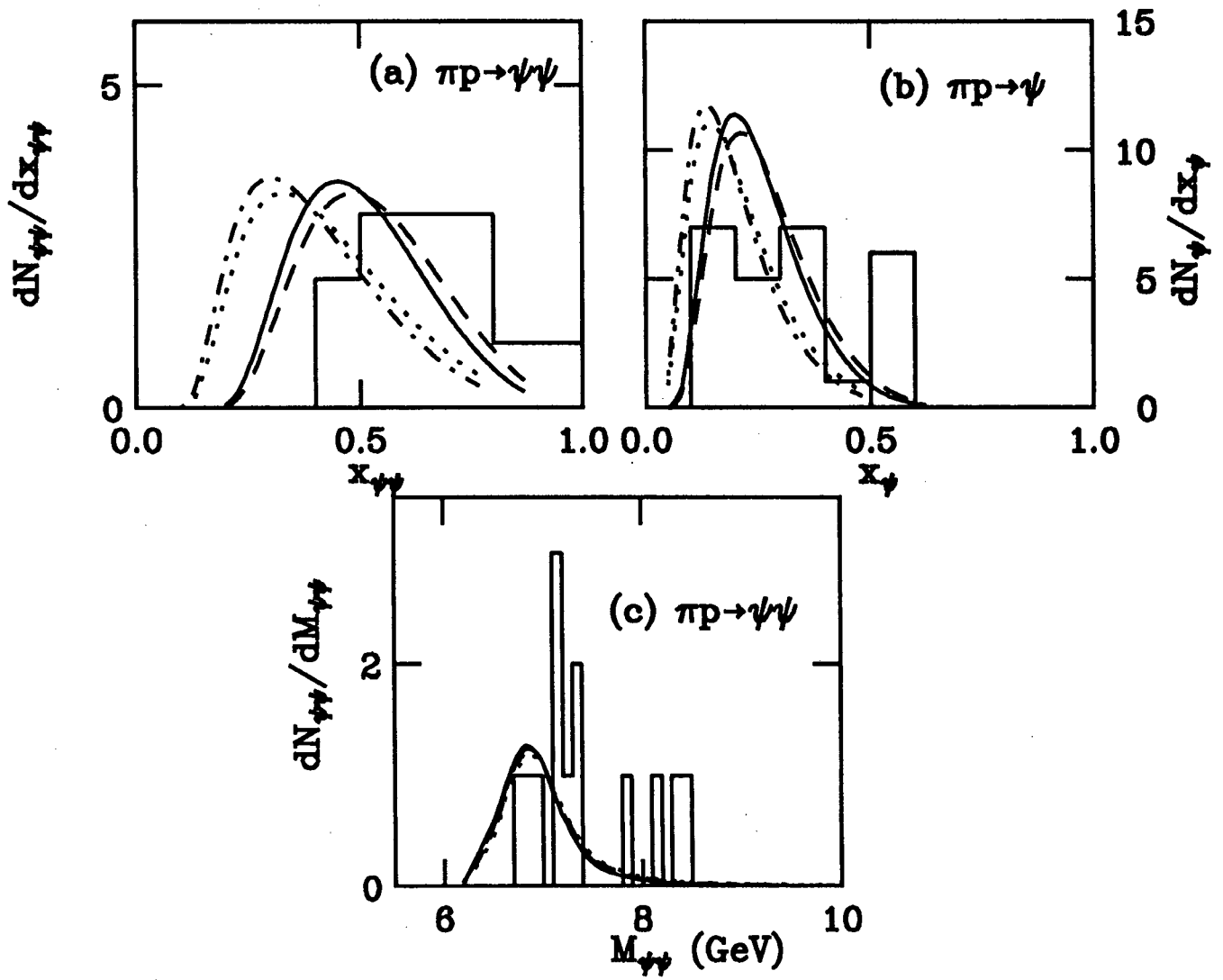
(a) πp→ψψ
(b) πp→ψ
(c) πp→ψψ
dN_ψψ/dx_ψψ
dN_ψ/dx_ψ
dN_ψψ/dM_ψψ
x_ψψ
x_ψ
M_ψψ (GeV)
0.0
0.5
1.0
0
5
10
15
2
6
8
10

Figure 7

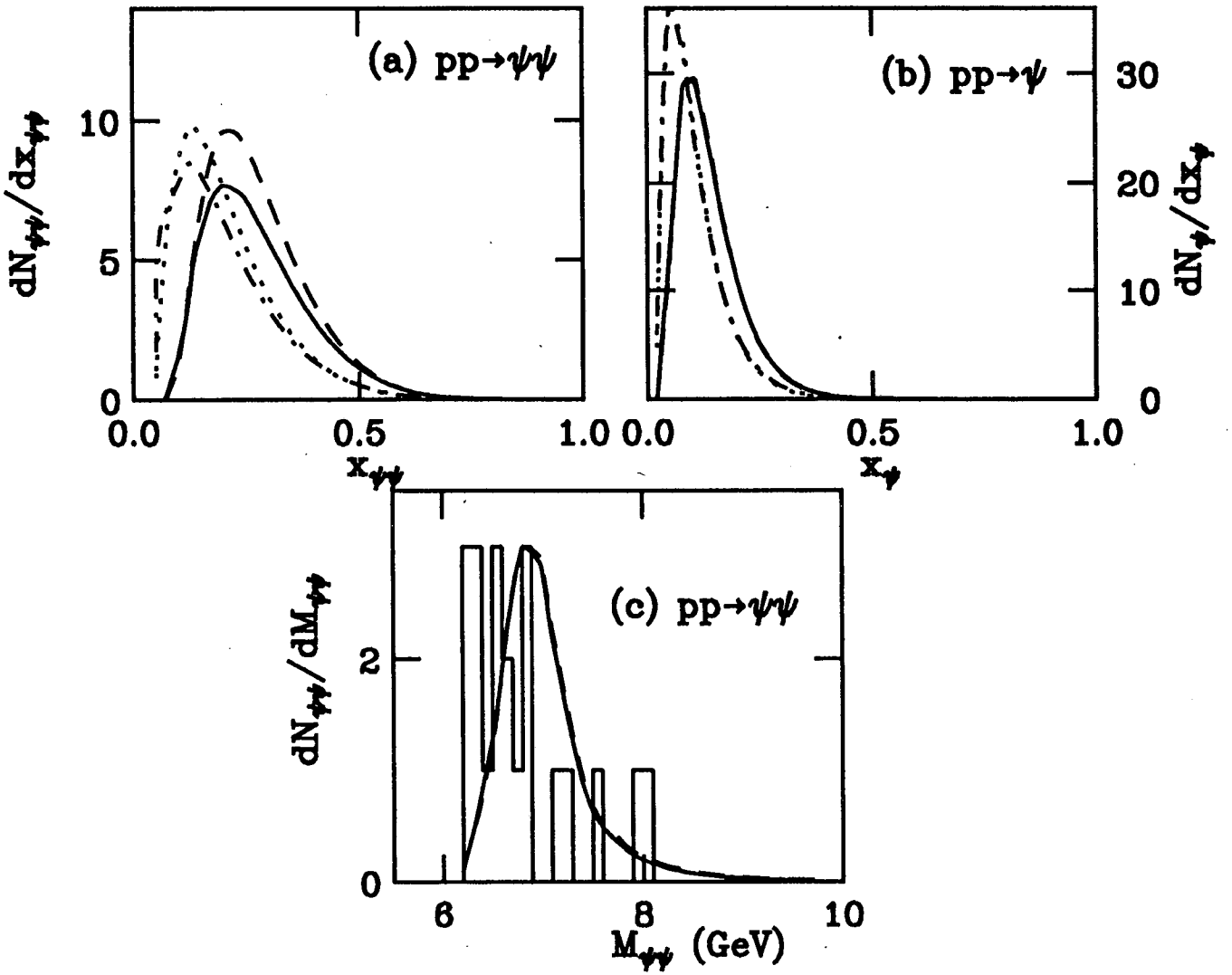
(a) pp→ψψ
(b) pp→ψ
(c) pp→ψψ
dN_ψψ/dx_ψψ
dN_ψ/dx_ψ
dN_ψψ/dM_ψψ
x_ψψ
x_ψ
M_ψψ (GeV)
0.0
0.5
1.0
0
5
10
20
30
2
6
8

Figure 8

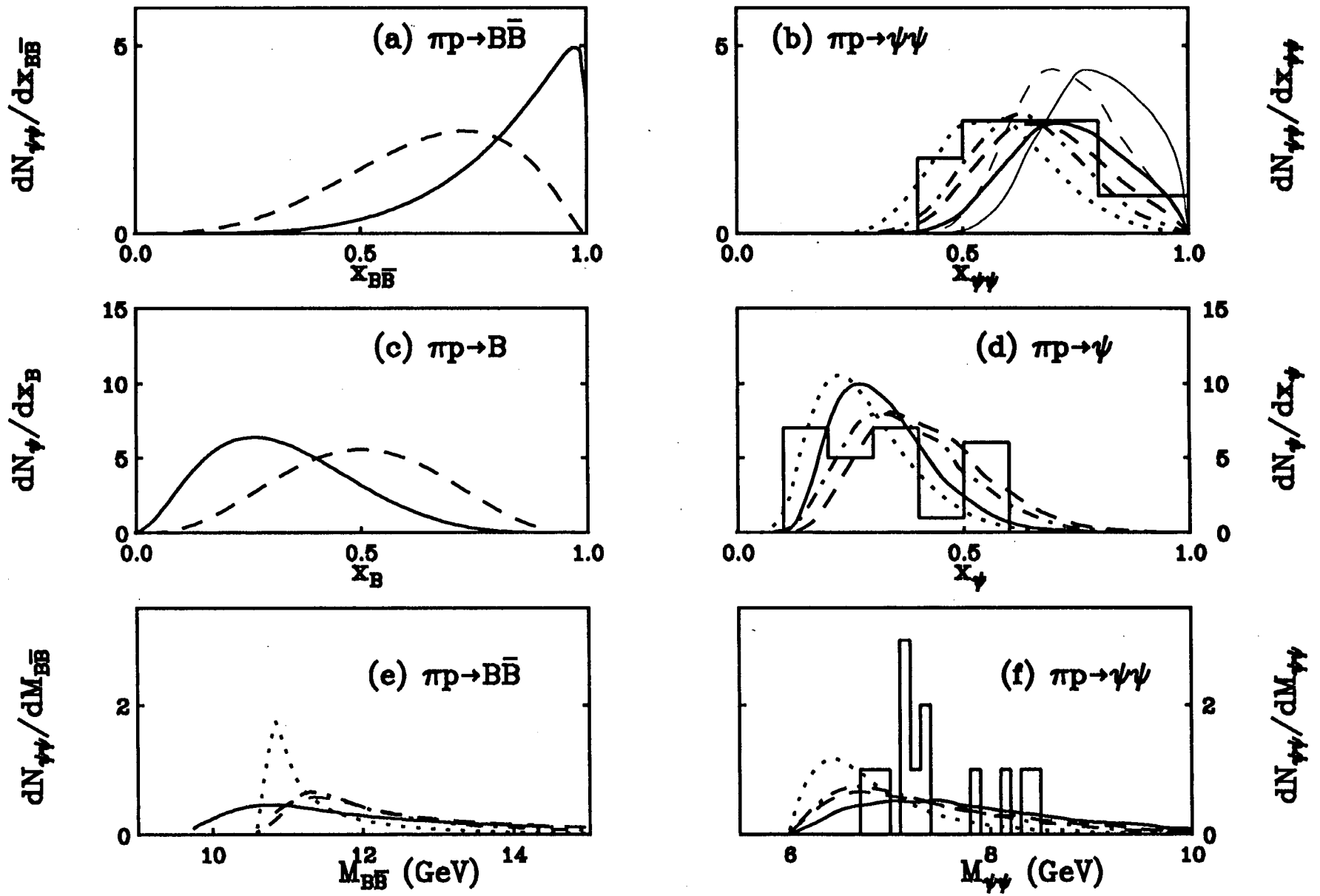
(a) πp→BB̄
(b) πp→ψψ
(c) πp→B
(d) πp→ψ
(e) πp→BB̄
(f) πp→ψψ
dN_ψψ/dx_BB̄
dN_ψψ/dx_ψψ
dN_ψ/dx_B
dN_ψ/dx_ψ
dN_ψψ/dM_BB̄
dN_ψψ/dM_ψψ
x_BB̄
x_ψψ
x_B
x_ψ
M_BB̄ (GeV)
M_ψψ (GeV)
0.0
0.5
1.0
0
5
10
15
2
6
8
10
12
14

Figure 9

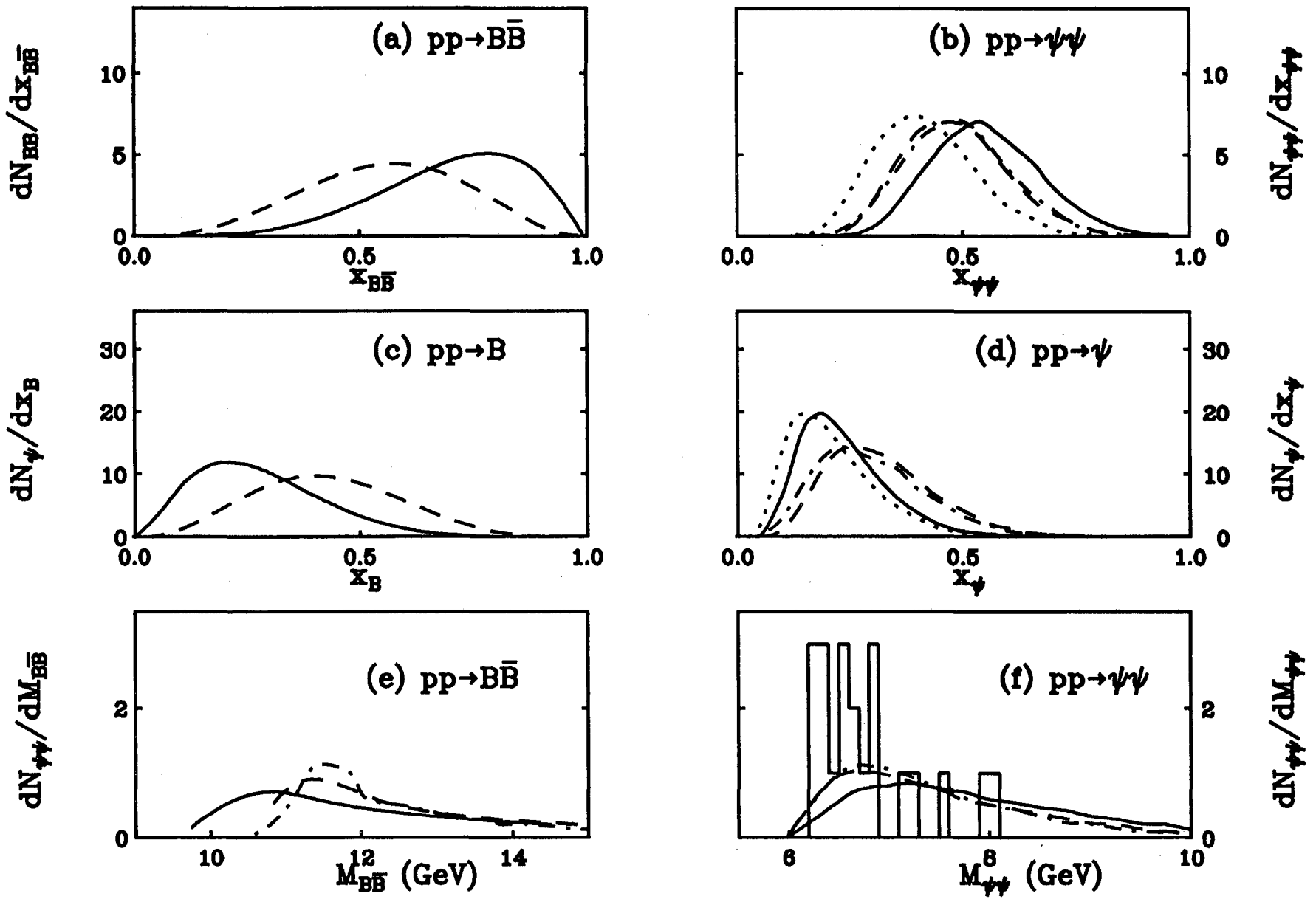
(a) pp→BB̄
(b) pp→ψψ
(c) pp→B
(d) pp→ψ
(e) pp→BB̄
(f) pp→ψψ
dN_BB̄/dx_BB̄
dN_ψψ/dx_ψψ
dN_ψ/dx_B
dN_ψ/dx_ψ
dN_ψψ/dM_BB̄
dN_ψψ/dM_ψψ
x_BB̄
x_ψψ
x_B
x_ψ
M_BB̄ (GeV)
M_ψψ (GeV)
0.0
0.5
1.0
0
5
10
20
30
2
6
8
10
12
14

Figure 10

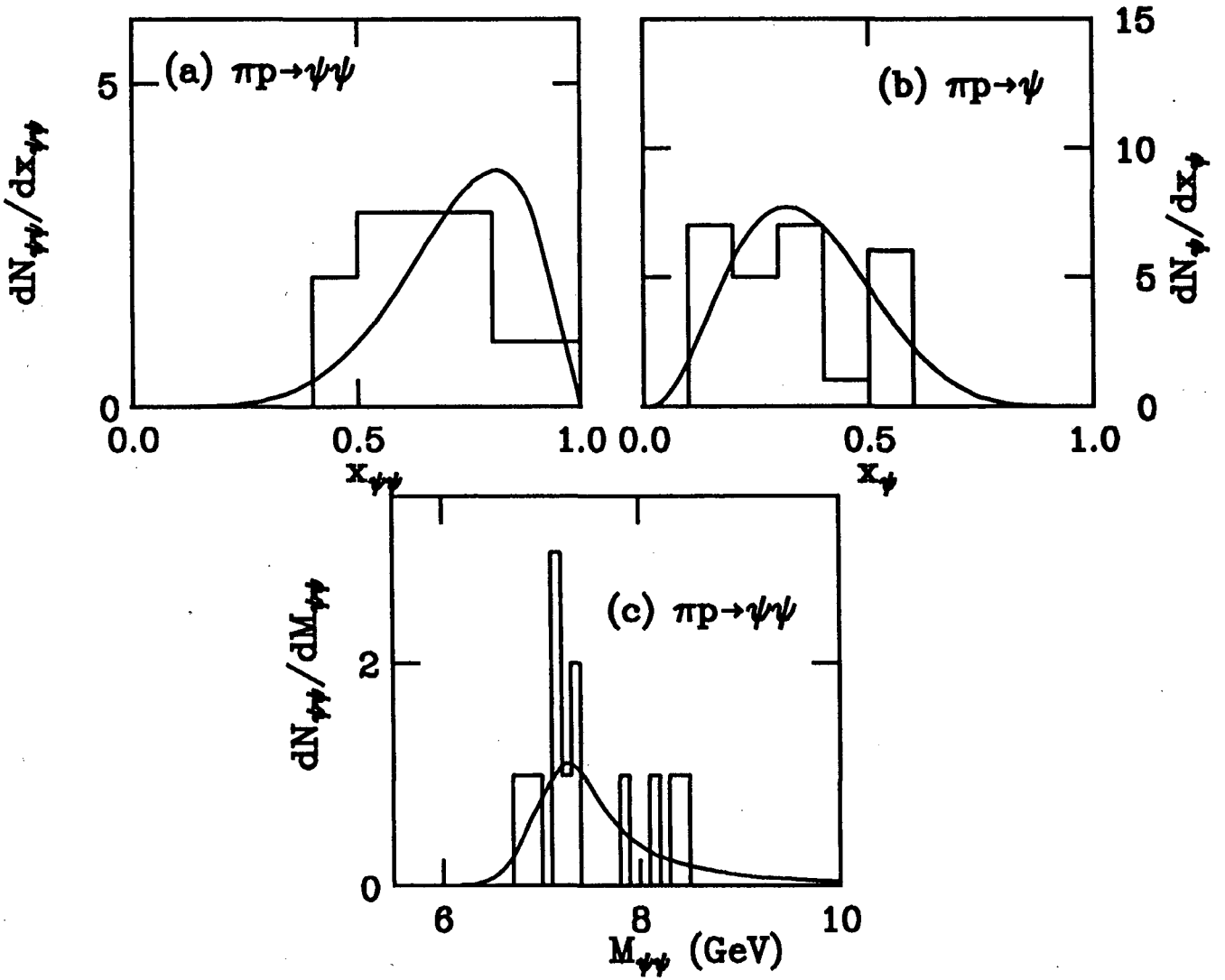
(a) πp→ψψ
(b) πp→ψ
(c) πp→ψψ
dN_ψψ/dx_ψψ
dN_ψ/dx_ψ
dN_ψψ/dM_ψψ
x_ψψ
x_ψ
M_ψψ (GeV)
0.0
0.5
1.0
0
5
10
15
2
6
8
10

Figure 11

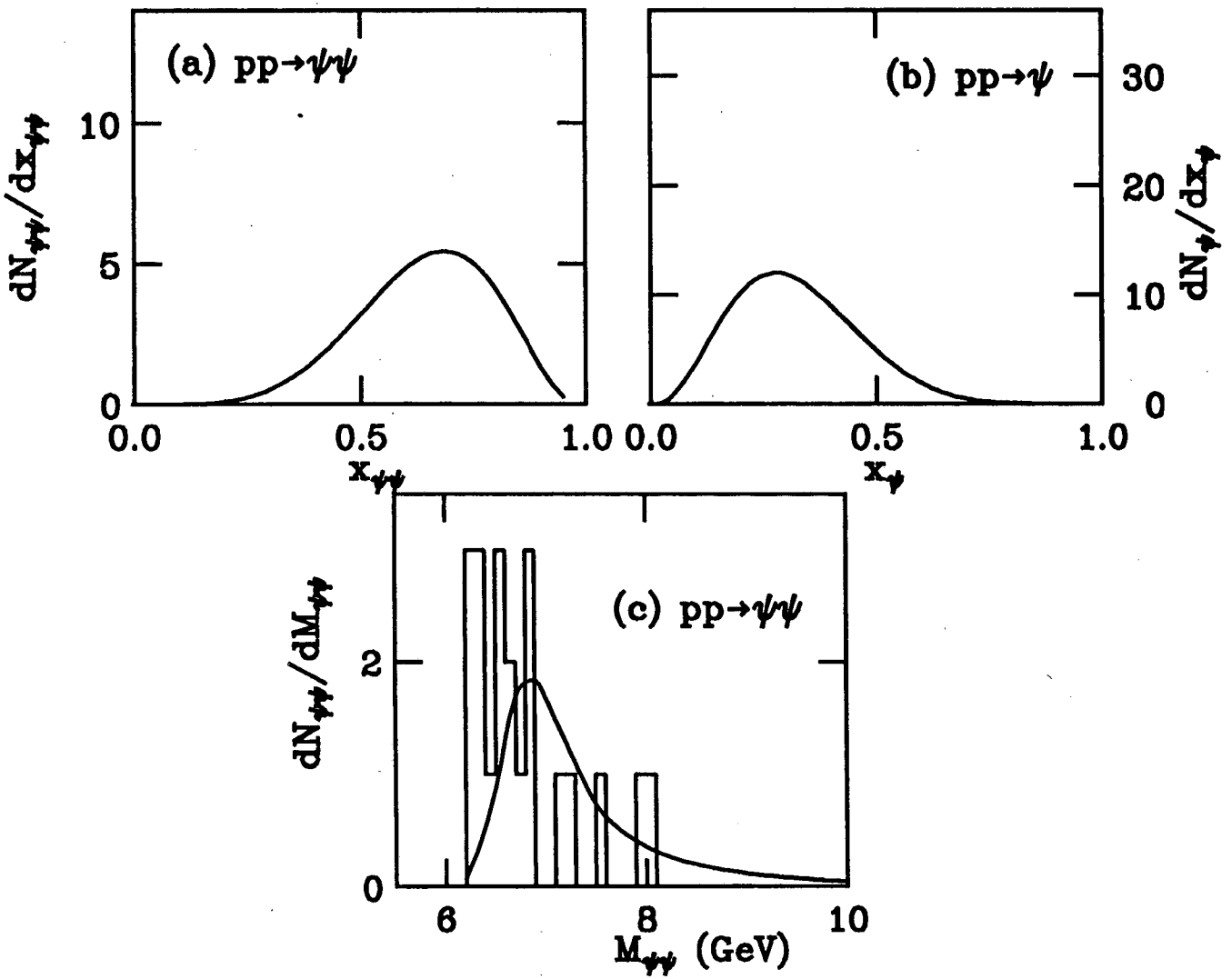
(a) pp→ψψ
dN_ψψ/dx_ψψ
0
5
10
0.0
0.5
1.0
x_ψψ
(b) pp→ψ
dN_ψ/dx_ψ
0
10
20
30
0.0
0.5
1.0
x_ψ
(c) pp→ψψ
dN_ψψ/dM_ψψ
0
2
6
8
10
M_ψψ (GeV)

Figure 12

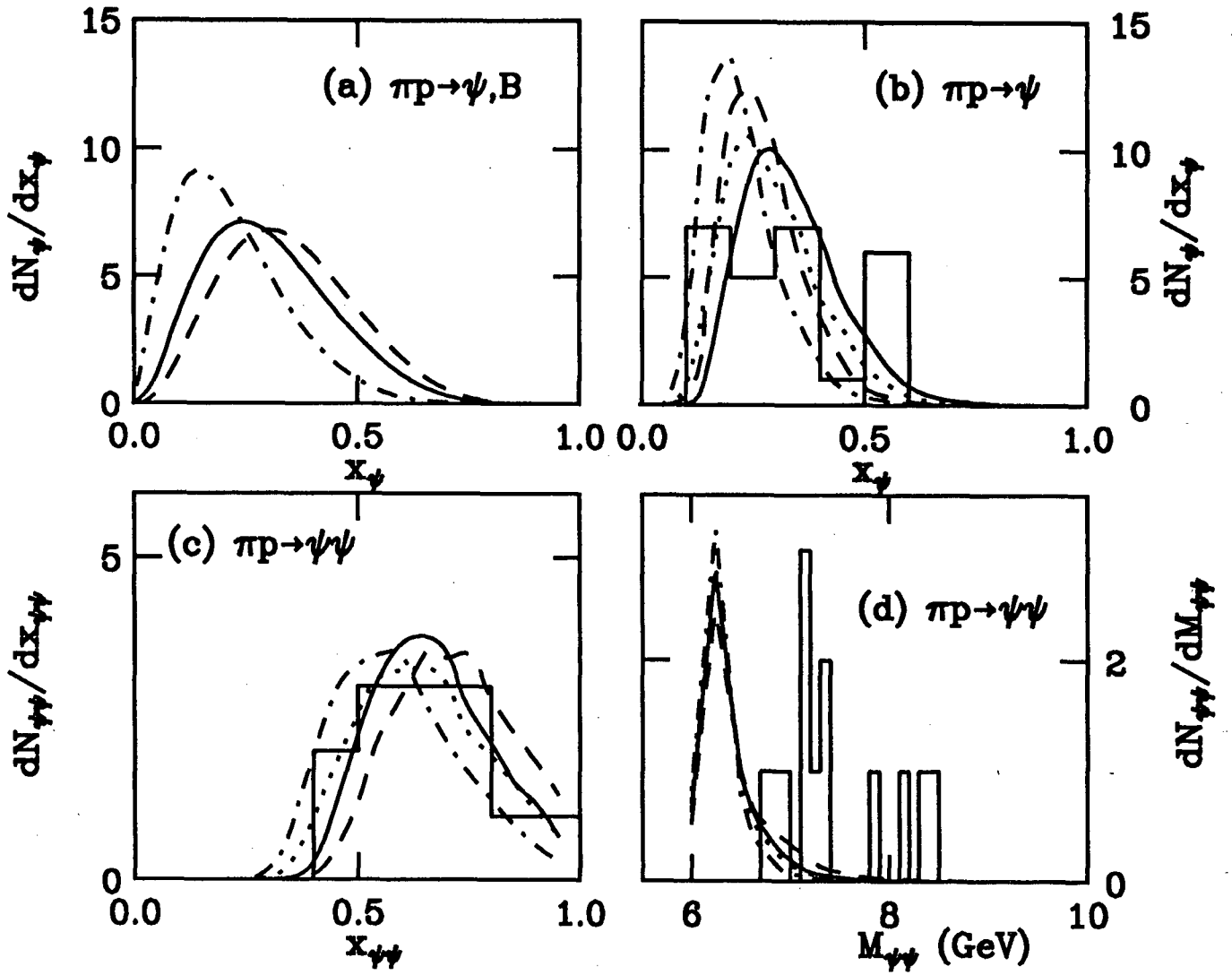
(a) πp→ψ,B
(b) πp→ψ
(c) πp→ψψ
(d) πp→ψψ
dN_ψ/dx_ψ
dN_ψψ/dx_ψψ
dN_ψψ/dM_ψψ
x_ψ
x_ψψ
M_ψψ (GeV)
0.0
0.5
1.0
6
8
10
0
5
10
15
2

Figure 13

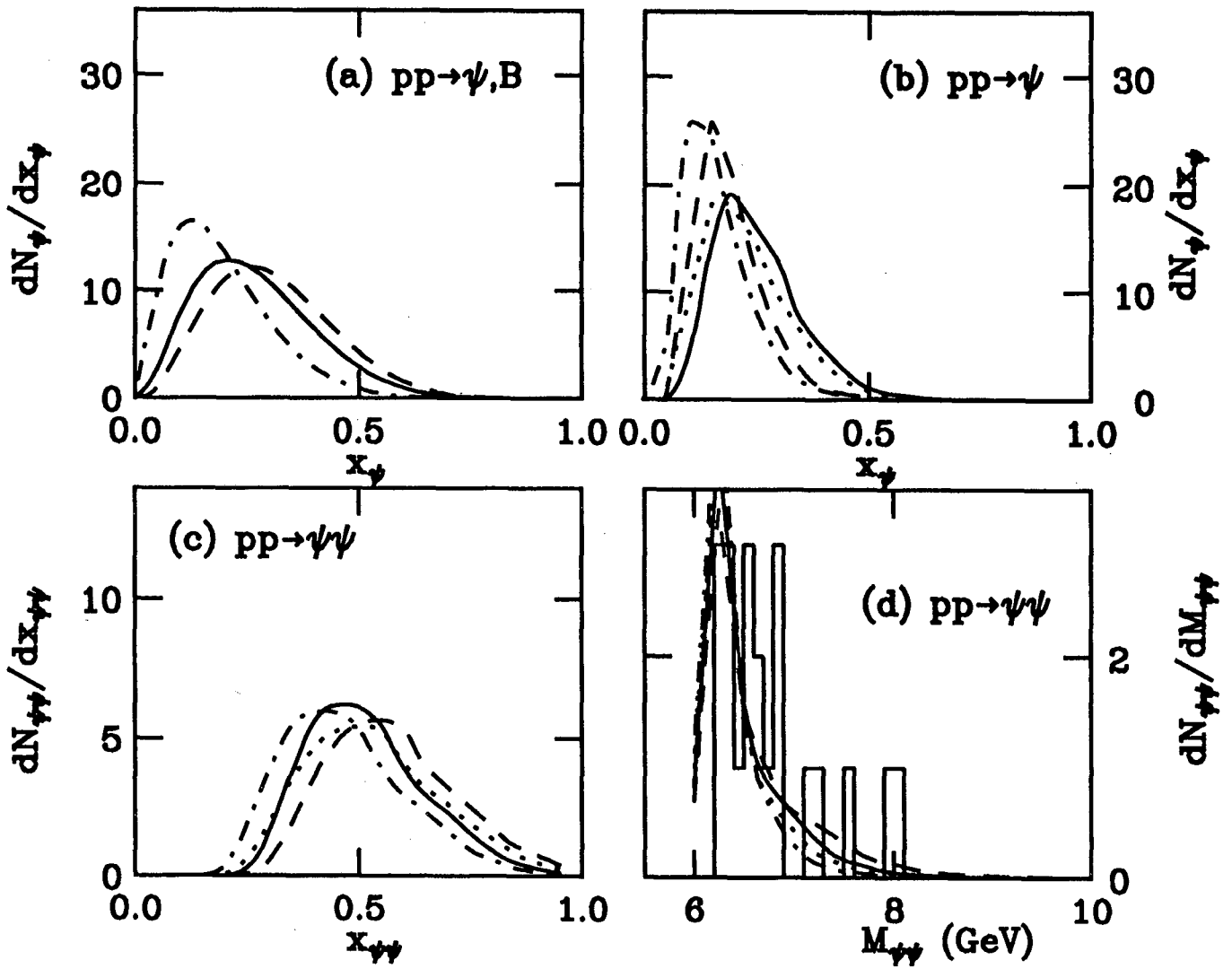
(a) pp→ψ,B
(b) pp→ψ
(c) pp→ψψ
(d) pp→ψψ
dN_ψ/dx_ψ
dN_ψψ/dx_ψψ
dN_ψψ/dM_ψψ
x_ψ
x_ψψ
M_ψψ (GeV)
0.0
0.5
1.0
6
8
10
0
10
20
30
5
2

Figure 14

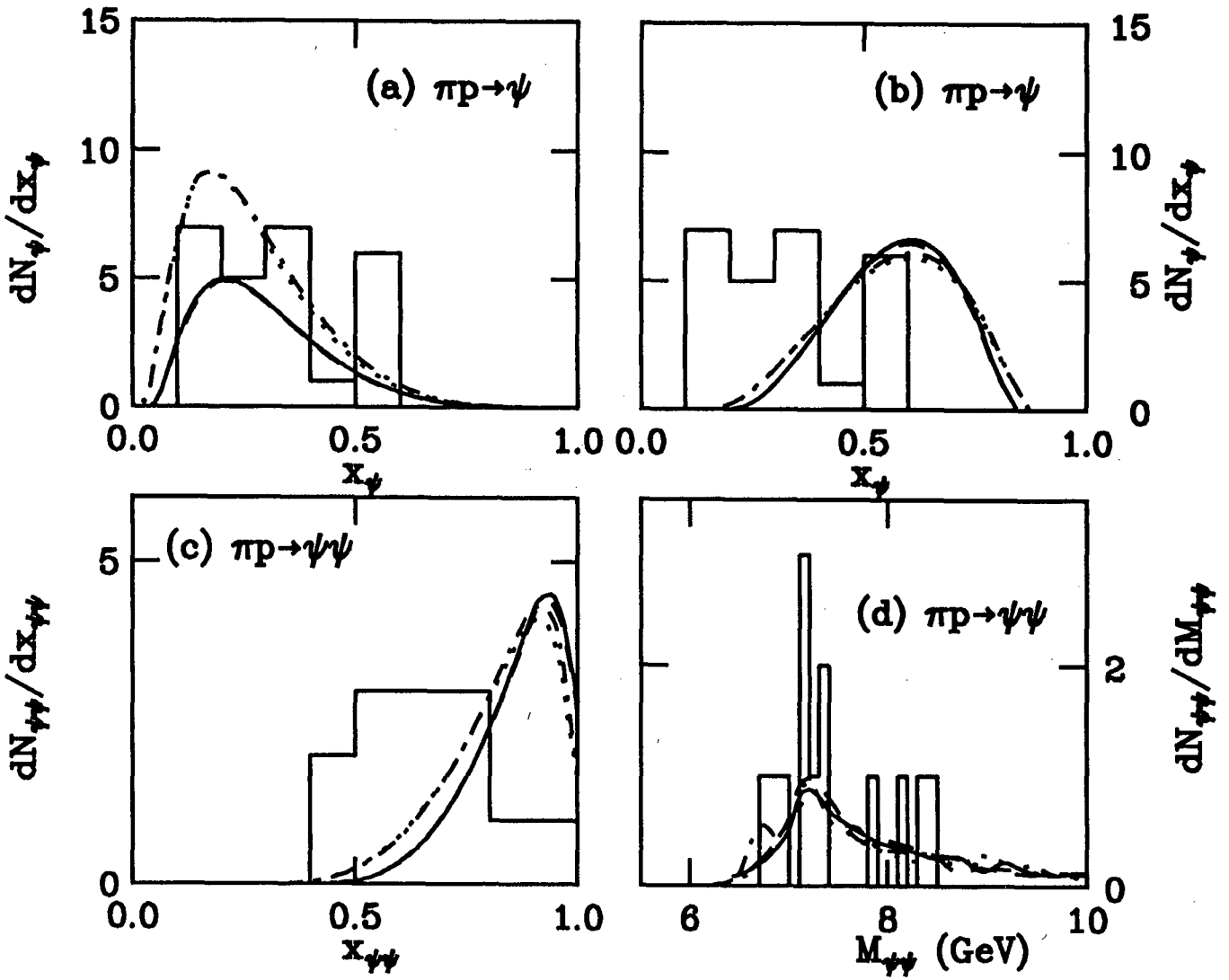
(a) πp→ψ
(b) πp→ψ
(c) πp→ψψ
(d) πp→ψψ
dN_ψ/dx_ψ
dN_ψψ/dx_ψψ
dN_ψψ/dM_ψψ
x_ψ
x_ψψ
M_ψψ (GeV)
0.0
0.5
1.0
6
8
10
0
5
10
15
2

Figure 15

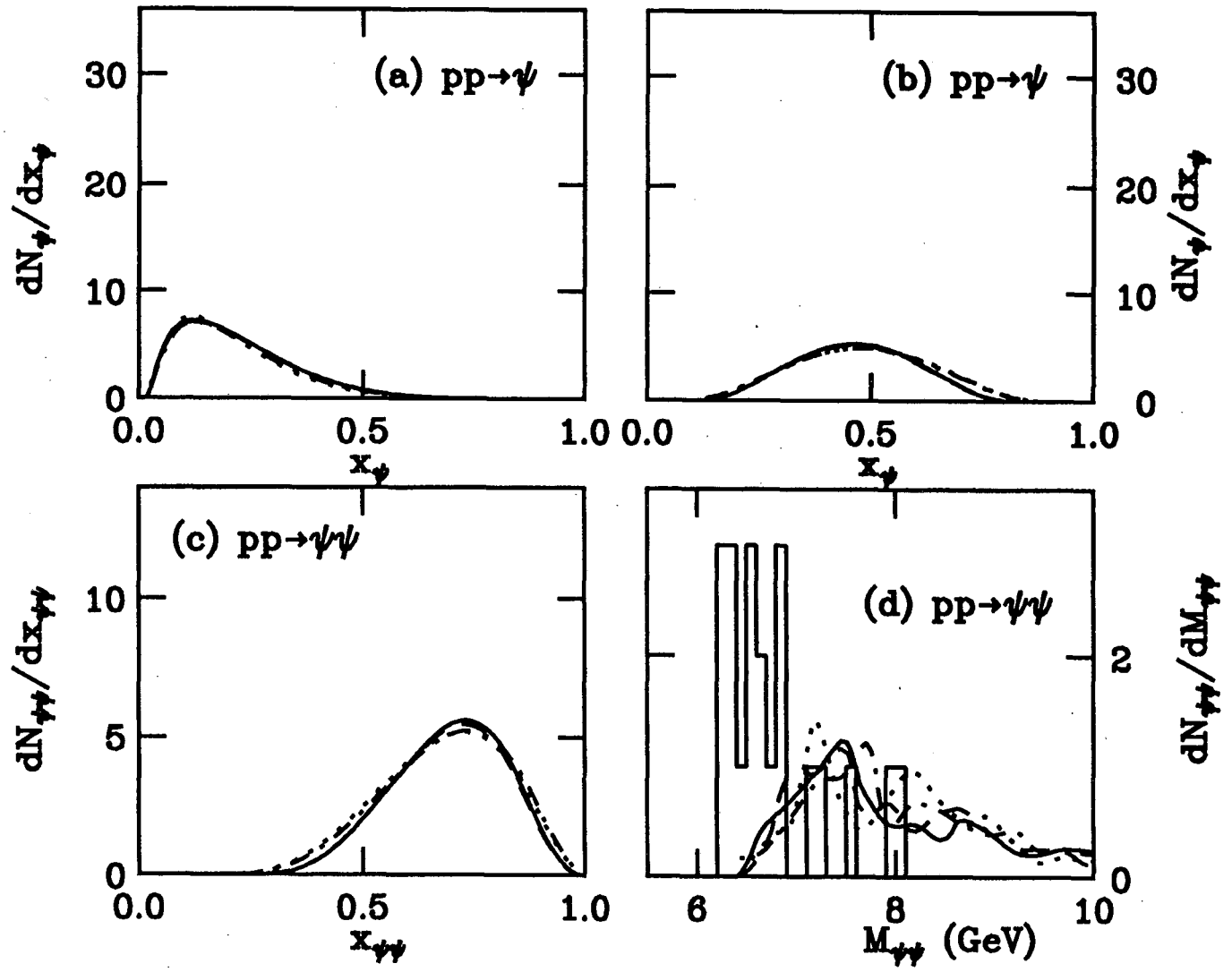
(a) pp→ψ
(b) pp→ψ
(c) pp→ψψ
(d) pp→ψψ
dN_ψ/dx_ψ
dN_ψψ/dx_ψψ
dN_ψψ/dM_ψψ
x_ψ
x_ψψ
M_ψψ (GeV)
0.0
0.5
1.0
6
8
10
0
10
20
30
5
2

LAWRENCE BERKELEY LABORATORY
UNIVERSITY OF CALIFORNIA
TECHNICAL AND ELECTRONIC
INFORMATION DEPARTMENT
BERKELEY, CALIFORNIA 94720